energies

Article

The Study on Diagenetic Characteristics of Coal Measures Sandstone Reservoir in Xishanyao Formation, Southern Margin of the Junggar Basin

Aobo Zhang [1,2], Shida Chen [1,2,*], Dazhen Tang [1,2,*], Shuling Tang [1,2], Taiyuan Zhang [1,2], Yifan Pu [1,2] and Bin Sun [3]

[1] School of Energy Resources, China University of Geosciences (Beijing), Beijing 100083, China; zhangaobo1994@outlook.com (A.Z.); tangshuling@cugb.edu.cn (S.T.); zhangtaiyuan@cugb.edu.cn (T.Z.); 3006200027@cugb.edu.cn (Y.P.)

[2] Coal Reservoir Laboratory of National Engineering Research Center of Coalbed Methane Development & Utilization, Beijing 100083, China

[3] Unconventional Research Institute, Research Institute of Petroleum Exploration and Development, Beijing 100083, China; sbin@petrochina.com.cn

* Correspondence: Shida.Chen@cugb.edu.cn (S.C.); tang@cugb.edu.cn (D.T.)

Abstract: The reservoir physical properties, pore types, diagenetic characteristics and reservoir quality controlling effect of the Xishanyao formation coal measure sandstone in the southern margin of the Junggar basin were discussed in this study based on thin section observation, high pressure mercury injection, low-temperature nitrogen adsorption and scanning electron microscope observation. The result shows that the porosity and permeability of the sandstone are generally low with a medium-high texture maturity and low compositional maturity. The sandstone storage space is mainly composed of residual intergranular pores, secondary dissolution pores, inter-crystalline pores and micro-fractures. The diagenetic stage of coal measure sandstone is in the mesodiagenesis A1-A2 stage, and their diagenetic interaction types mainly include compaction, cementation and dissolution. The reservoir quality of the coal measure sandstone deteriorates by compaction due to high matrix content and plastic debris content. Because of the large amounts of organic acids generated during the thermal evolution of the coal measure source rock, the coal measure sandstone suffers from strong dissolution. The secondary dissolution pores formed by the massive dissolution of feldspar, lithic fragments and early carbonate cementation in the sandstone significantly improved the reservoir quality. In the coal measure sandstone, clay mineral cementation is the most developed cementation form, followed by quartz cementation and carbonate cementation. Although kaolinite cementation and dolomite cementation can generate a small number of inter-crystalline pores, cementation deteriorates the reservoir quality. The Xishanyao formation coal measure sandstone formed in a lacustrine-delta environment, and its composition and texture make it susceptible to the influence of compaction and dissolution during diagenesis.

Keywords: tight sandstone; coal measure; southern margin of Junggar basin; diagenetic process; reservoir quality control; reservoir forming

check for updates

Citation: Zhang, A.; Chen, S.; Tang, D.; Tang, S.; Zhang, T.; Pu, Y.; Sun, B. The Study on Diagenetic Characteristics of Coal Measures Sandstone Reservoir in Xishanyao Formation, Southern Margin of the Junggar Basin. *Energies* **2022**, *15*, 5499. https://doi.org/10.3390/en15155499

Academic Editor: Rajender Gupta

Received: 29 June 2022
Accepted: 26 July 2022
Published: 29 July 2022

1. Introduction

The Junggar basin is abundant in coalbed methane (CBM) resources, of which the predicted resource of CBM with a burial depth of less than 2000 m is 3.11×10^{12} m^3, and the southern margin of the Junggar basin (SJB) has the best preservation conditions for CBM [1]. The main coal-bearing strata in the SJB are lower-middle Jurassic, and the sedimentary environment mainly includes alluvial fans, fan deltas, braided river deltas, and shore shallow lakes [1–3]. The SJB has characteristics of thick and multiple coal seams developed with a laterally widely distribution and frequent interbedded sandstone, shale, and coal seams in the vertical direction which is favorable for the co-accumulation of coal measure gases [4–10] (CMG, including CBM, coal measure tight sandstone gas and coal measure shale gas). The precedent of successful development in the Ordos basin [5,11,12] and the maturation of CMG symbiotic accumulation theory [7,8] have made the industry aware of the great potential in CMG development. The reservoir quality is crucial for the efficient development of coal measure tight sandstone gas, and regional differences in diagenetic environment and tectonic events lead to different factors affecting reservoir quality [13–19]. In order to efficiently develop the abundant tight sandstone that is contained in the coal measures in the SJB, it is necessary to conduct research on the petrological characteristics and reservoir quality of coal measures sandstone.

The tight sandstone reservoirs generally undergo a complex diagenesis process, resulting in progressive tightness during burial and thermal evolution [13–18]. The effects of reservoir quality include sedimentary, diagenesis and epigenesis, and the specific influencing factors include clastic composition, depositional environment, sedimentary facies, burial temperature and pressure [19,20]. Sedimentation controls the grain size, sorting, and arrangement of particles, as well as the mineral transformation and sedimentary structure [16,21–23]. The influence of diagenesis on the sandstone is mainly in terms of temperature, pH, pressure, etc., and is presented in the form of compaction, dissolution, cementation, and metasomatism [19,21,24]. Compaction is one of the main factors leading to the reduction of porosity and permeability [25], and the reservoir quality is particularly affected by the degree of compaction and the content of plastic particles (such as lithic fragments, mica, argillaceous debris) and matrix [19,26]. Cementation generally leads to the plugging of pore throats and seriously reduces permeability [27–32], but at the same time, it can also restrain the deterioration of reservoir quality to a certain extent: The inter-crystalline pores formed by the clay minerals cementation can provide storage space for sandstones [31,33,34]; the clay film covering the particle surface resists compaction and inhibits the development of other types of cement [13,35], thereby preserving residual pores; the clay film coating the particle surface can resist compaction and inhibit the development of other types of cement; the quartz cementation and carbonate cementation in the eodiagenesis can improve the compaction resistance ability of sandstone [15,36,37]. By analyzing the sedimentary environment, composition, and diagenesis characteristics of the coal measure sandstone, the reservoir quality control factors of the coal measure sandstone in the Xishanyao formation can be clarified and the formation and evolution process of the coal measure sandstone reservoir can be explained.

The coal seams of the Xishanyao formation on the southern margin of the Junggar basin are mainly in the low-medium coal rank, with frequent interbedding of sandstones, mudstones and coal seams [1]. The diagenesis of coal measure sandstone is strongly influenced by the thermal evolution of coal seams and dark shale [7,8]. Previous studies on sandstone reservoirs have mainly focused on the mechanism of pore throat formation, quantitative characterization of pore throats, and the relationship between oil and gas intrusion and reservoir diagenesis of sandstone reservoirs in different zones or layers within the basin [38–43]. However, studies on the coal-bearing sandstones of the Middle Jurassic Xishanyao formation have also focused on the evolution of the sedimentary environment, the classification of reservoir types, and the classification and evaluation of reservoirs [2,4,44–47]. As the understanding of the diagenetic sequence of the coal measure sandstone reservoirs in the Xishanyao formation, and the influence on reservoir quality is not comprehensive enough, it is urgent to carry out relevant work. This paper combined techniques including casting thin section observation, scanning electron microscope (SEM), XRD experiment, high-pressure mercury intrusion, low-temperature nitrogen adsorption, and Ro test of coal measure shale to conduct research on the following contents: (1) Determine the characteristics of coal measure sandstone in the Xishanyao formation; (2) clarify the diagenetic evolution sequence of coal measure sandstone in the Xishanyao formation; (3) clarify the controlling effect of sedimentation and diagenesis on the reservoir quality of coal measure sandstone. This study is expected to provide a reference for the exploration and development of tight sandstone gas in the Xishanyao formation coal measures.

2. Geology Background

The Junggar basin is located in the northern part of Xinjiang; it is a large-scale Mesozoic-Cenozoic depression basin with an area of about 13.4 × 10^4 km^2 and an approximately triangular shape in the plane, with a width of 1120 km from east to west and 800 km from north to south [1–3]. Since the Late Paleozoic, the Junggar basin has experienced Hercynian, Indosinian, Yanshan and Himalaya tectonic movements, and the superposition of multi-phase stress fields has led to its structural complexity [2,44,48]. The Junggar basin can be divided into six structural units: the Luliang uplift, the Ulungu depression, the northern Tianshan piedmont thrust belt, the western uplift, the central depression, and the eastern uplift [3,49] (Figure 1A). The SJB is located in the northern Tianshan piedmont thrust belt, which elongates east-west direction with a north-south width of nearly 200 km (Figure 1B). The northern Tianshan piedmont thrust belt is a multi-phase superimposed and inherited structural belt, and is usually divided into five secondary structural units, including the Sikeshu sag, Qigu fault–fold belt, Huomatu anticlinal zone, Huan anticlinal zone, and Fukang fault zone [50].

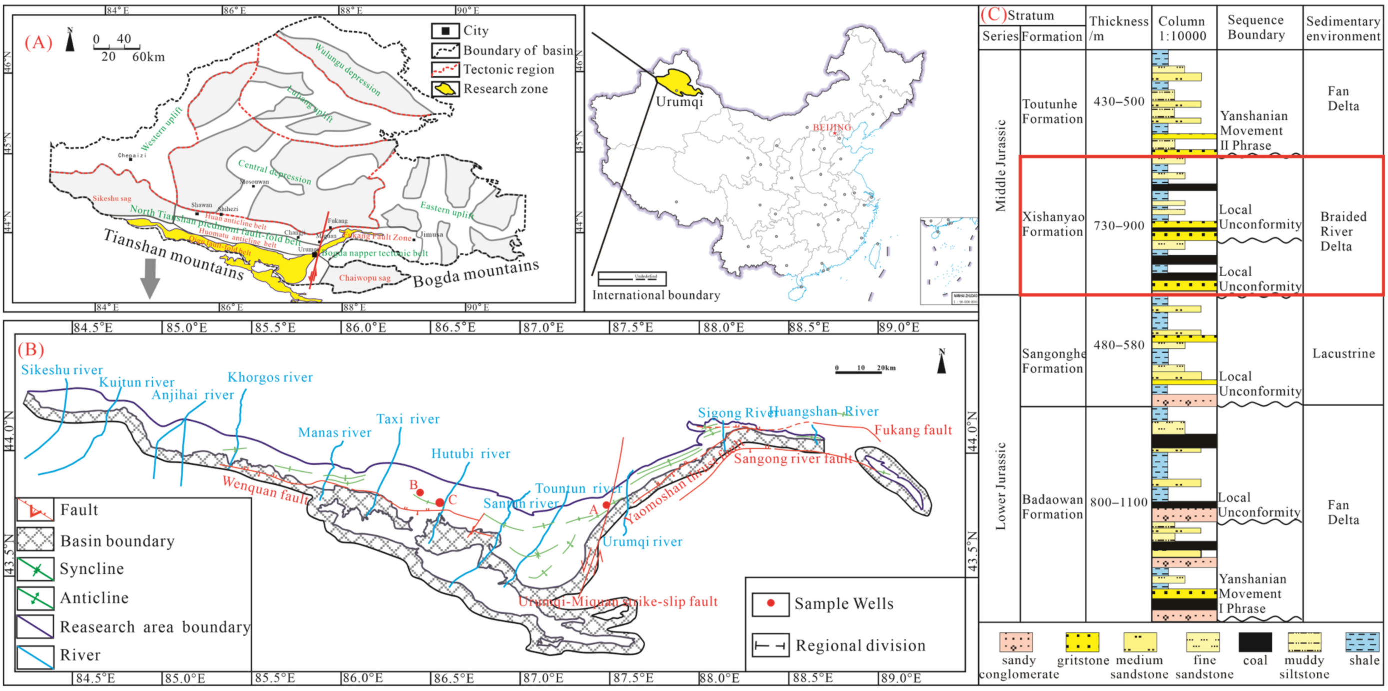

Figure 1. Maps showing: (**A**) Location of the Junggar basin in China (modified by [4]). (**B**) Structural outline map (modified by [10,51]) of the Southern margin of Junggar basin (SJB). (**C**) The stratigraphic column shows the Middle-lower Jurassic Strata in SJB (modified by [51], Xishanyao formation is marked in red).

A major part of the surface of the SJB is covered by quaternary strata. The strata in the SJB area are Permian, Triassic, Jurassic and Palaeocene from old to new (Figure 1C). Among them, the Badaowan formation and Xishanyao formation are the main coal-bearing strata in the study area, which are widely distributed in the SJB (Figure 1C). The coal-bearing strata of the Xishanyao formation were formed in a lacustrine–deltaic sedimentary system [2,3]. The Xishanyao formation strata had multiple coal accumulation centers that were greater than 40 m thick between the present-day Horgos River and Sigong River controlled by tectonic and sedimentary conditions [1].

3. Materials and Methods

Overall, a total of 45 sandstone core samples from three wells in the Xishanyao formation in the SJB were collected and tested (Figure 1B). In addition, 16 shale samples were selected for vitrinite reflectance (Ro) testing to determine diagenetic evolution stages.

3.1. Mineral Composition and Morphology Analysis

A total of 43 casting thin sections were made and placed under a ZEISS Axio Imager II microscope for observation and analysis of the mineral petrological characteristics and pore structure characteristics. What is more, those thin sections have performed image particle size analysis following China's oil and gas industry standard SY/T 5434-2018.

The Scanning Electron Microscope (SEM) observation has been performed on seven sandstone samples by the ZEISS EVO MA 15 scanning electron microscope to clarify their mineral types, pore structure and diagenetic characteristics.

The whole-rock and clay mineral analyses (X-ray diffraction, XRD) were performed on 16 sandstone samples (Table 1) by Rigaku TTR III diffractometer (40 kV, 200 mA and a step size of 8° per minute) equipped with a Cu-Kα radiation source (λ = 1.541841 Å) following the Chinese oil and gas industry standard SY/T 5163-2010.

3.2. Petrophysical Parameters Analysis

The porosity and permeability tests were conducted on 21 sandstone samples (Table 2) using a CoreLab CAT-113 He-porosimeter and a CoreLab CAT-112 gas permeameter, respectively, according to Chinese oil and gas industry standard SY/T5336-2006.

3.3. Pore Structure Characterization Tests

The high-pressure mercury intrusion experiments (HPMI) were carried out on 27 samples by a Micromeritics Autopore IV 9505 instrument to characterize the complexity and heterogeneity of the pore throat structure (Table 2) following the China Petroleum and Natural Gas Industry Standard SY/T 5346-2012. The instrument automatically records the pressure, pore size, intrusion volume and surface area with the increase in the mercury injected amount.

The low-pressure N_2 gas adsorption (N_2GA) experiments were conducted on 23 crushed sandstone samples (Table 2) using V-Sorb 2800P series specific surface area and pore size analyzers (temperature 77 K, pressure < 127 kPa). The specific surface area and total pore volume were calculated using the BET model [52] and the BJH model [53] according to the N_2GA data, respectively.

Table 1. The result of XRD experiments of sandstones in the Xishanyao formation.

Well	Strata	Depth (m)	Whole Rock (%)									Clay Mineral (%)					
			Quartz	K-Felspar	Plagioclase	Calcite	Dolomite	Apatite	Ankerite	Siderite	Clay Mineral	S	I/S	Illite	Kaolinite	Chlorite	C/S
A	J_2x	303	54.3	5	25.5			1.2			14		62	36	2		
A	J_2x	601	50	0.6	16.6						32.8		62	15	23		
A	J_2x	653.5	43.6	0.2	21			1.1			34.1		50	16	34		
A	J_2x	669	43.3	0.5	10					15.9	30.3		61	15	24		
A	J_2x	673	38.4	0.7	16.4			4.5			40		48	26	26		
B	J_2x	919	48.6	3.1	14			8.5			25.8		31	39	23	7	
B	J_2x	922.5	47.9	9.9	19.1			6.7			16.4		23	32	40	5	
B	J_2x	935	41.1	10.8	22.9			7.2			18		25	32	43		
B	J_2x	994.5	61.5	1.2	29.1	2					6.2		38	17	35	10	
B	J_2x	1055	48.2	7.6	29.7						14.5		43	30	27		
B	J_2x	1090	41.5	8.3	15.3		10.4		12		12.5		20	30	50		
C	J_2x	967	44.9	12.2	25.3			2.6			15		16	34	50		
C	J_2x	987	41.7	7.8	15.7		10	4.8			20		15	32	47	6	
C	J_2x	988	43.4	6.2	17.4		23.8	1.6			7.6		17	39	44		
C	J_2x	1011	50.1	6.4	16			2.8			24.7		24	38	38		
C	J_2x	1061	58.7	11.6	17.7			0.5			11.5		25	32	43		

Table 2. The physical properties and pore structure characterization of coal measure sandstones in the Xishanyao Formation.

Well	Depth	Sorting Efficient	Matrix Content (%)	Mean Grain Size (mm)	Permeability (mD)	Porosity (%)	Pore Throat Radius (μm)		Maximum Injected Mercury Saturation (%)	Mercury Withdrawal Efficiency (%)	Pore Volume ($\times 10^{-5}$ mL/g)			Specific Surface Area (m^2/g)
							Mean Value	Median Value			Micropores	Mesopores	Macropores	
A	303	1.211	4.5	0.203	0.53900	7.481	0.319	0.241	95.00	55.86	52	269	138	1.242
A	305	1.264	4.5	0.225							36	308	99	1.062
A	305.61	1.232	4.2	0.241										
A	308	1.806	4.2	0.274	0.15270	10.86					43	252	128	0.982
A	355	1.931	10.5	0.035			0.616	0.331	95.96	51.51				
A	380	1.381	8.5	0.048										
A	404	1.273	4	0.153										
A	407.05	1.056	5	0.116										
A	507.4	0.933	5	0.098										
A	573	0.973	5	0.114										
A	601				0.00039	3.476	0.012	0.010	95.05	47.92	214	1348	313	6.099
A	653.5	1.248	10	0.071	0.00068	4.058	0.015	0.012	91.93	40.28	167	967	227	4.905
A	655	0.707	9	0.041										
A	669						0.012	0.008	91.27	49.21	175	1050	295	5.124
A	670	1.252	20	0.028										
A	673	1.246	20	0.033			0.015	0.012	94.79	42.01	244	1091	325	6.53
B	841	1.258	4	0.301										
B	889.9	0.723	4	0.222										
B	919	1.283	8	0.087	0.00154	1.889	0.037	0.022	85.18	55.95	43	295	57	1.15
B	921	0.838	3.8	0.118	0.00600	1.400	0.050	0.029	89.89	53.23				
B	922	1.239	10	0.081										
B	922.5	1.411	15	0.054			0.013	0.006	75.05	73.00	43	265	62	0.93
B	934.1	0.816	4	0.161										
B	935	1.164	8	0.080	0.00016	1.30	0.015	0.006	65.74	57.21	32	134	69	0.64
B	937.5	1.079	8	0.131			0.088	0.015	71.34	65.06	27	159	52	0.51
B	968.7	1.282	4.5	0.148										
B	987	1.348	5	0.131	0.00710	1.93	0.081	0.044	88.09	56.03	30	147	37	0.54
B	1018.5	0.996	4.5	0.181										
B	1034	1.080	3.5	0.274	0.04400	3.91	0.162	0.080	93.50	34.31				
B	1055	0.992	4	0.386	0.28900	3.11	0.413	0.124	91.23	51.48	44	239	161	0.77
B	1090	0.896	4.5	0.136	0.00320	1.68	0.010		34.91	25.29	23	176	56	0.41
B	1091	0.897	15	0.062	0.00280	1.38					60	366	103	1.50

Table 2. *Cont.*

Well	Depth	Sorting Efficient	Matrix Content (%)	Mean Grain Size (mm)	Permeability (mD)	Porosity (%)	Pore Throat Radius (μm)		Maximum Injected Mercury Saturation (%)	Mercury Withdrawal Efficiency (%)	Pore Volume ($\times10^{-5}$ mL/g)			Specific Surface Area (m^2/g)
							Mean Value	Median Value			Micropores	Mesopores	Macropores	
C	967	0.757	4	0.167	0.16100	5.03	0.233	0.134	94.28	48.85	59	220	75	1.33
C	970.2	0.784	3.5	0.199	0.09800	4.65	0.195	0.155	94.18	39.73				
C	984	0.800	6.5	0.146	0.06200	2.37	0.091	0.050	92.75	34.68	41	262	175	0.92
C	984	1.384	5	0.168			0.229	0.075	95.72	53.83				
C	987	0.855	4.6	0.158	0.02430	3.75	0.112	0.050	92.35	47.85	46	258	109	1.05
C	988	0.875	4.5	0.168			0.076	0.023	91.57	50.46	36	145	46	0.64
C	988.5	1.471	7.8	0.135	0.01700	2.32	0.070	0.039	96.19	36.86				
C	991	1.111	15	0.026	3.42200	1.51								
C	994	0.900	5.2	0.039	0.00300	1.25	0.011	0.006	77.98	39.81				
C	1011	0.961	5	0.091	0.00469	4.87	0.042	0.015	91.39	73.21	43	289	170	0.79
C	1046	0.917	4	0.240	0.11680	2.73	0.134	0.039	93.33	53.09	53	365	94	1.49
C	1047	0.935	4.2	0.223			0.209	0.064	91.84	40.24	61	282	112	1.36
C	1061	0.873	4	0.415	0.20200	3.26	0.334	0.096	89.98	52.25	26	152	60	0.78

4. Results

4.1. Composition and Texture of Sandstone

The sandstone of the Xishanyao formation in the SJB is mainly feldspar lithic sandstone [47], and its compositional maturity is relatively low. The provenance of coal measure sandstone reservoirs comes from the Tianshan Mountains, and the parent rock types are middle-low-grade metamorphic rocks and middle-acid magmatic rocks [46,54].

According to the results of the image particle size analysis experiment. The particle size of sandstone is concentrated between silt and medium grains (mean grain size is 0.026–0.415 mm, Figure 2C), with a poor to medium sorting degree (sorting coefficient is 0.707–1.931), sub-angular to sub-round particle roundness, and high matrix content (3.5–20%, avg on 6.8%, Table 2). This evidence indicates that the texture maturity of coal measure sandstone is medium-high mature.

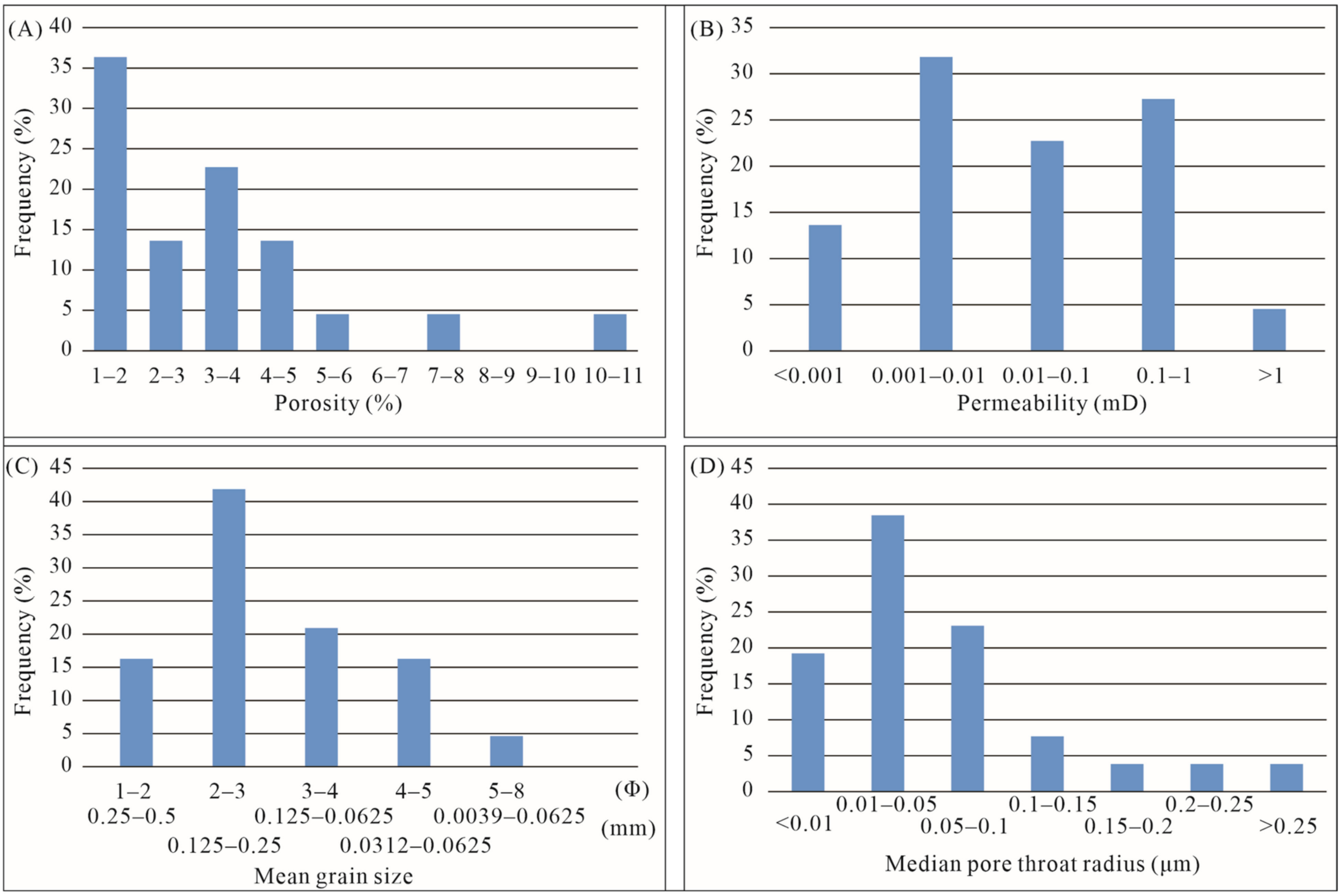

Figure 2. Frequency distribution histogram of porosity (**A**), permeability (**B**), average grain size (**C**) and median grain size radius (**D**).

The proportion of detrital particles in coal measure sandstone was analyzed through an XRD experiment: the content of quartz in the detrital grains was the highest, ranging from 38.4% to 61.5% (avg 47.3%); feldspar minerals included plagioclase and K-feldspar. Plagioclase content is slightly higher than K-feldspar, which is in the range between 10 and 29.7% (avg 19.5%); K-feldspar content is between 0.2 and 12.2% (avg 5.8%); apatite can be detected in many samples, and its content is between 0.5 and 8.5% (avg 3.5%); some samples can detect dolomite (shows in three samples, accounting for 10–23.8%), ankerite (shows in one sample, accounting for 12%) and siderite (shows in one sample, accounting for 15.9%); clay mineral content is between 2.0 and 29.8% (avg 7.8%).

The XRD test results of clay minerals show that the relative contents of clay minerals in the Xishanyao formation coal measure sandstone (Figure 3, Table 1): the content of illite is between 15 and 39% (avg 28.9%); the content of illite/smectite (I/S) mixed layer is between 15 and 62% (avg 35%); the kaolinite content is between 2 and 50% (avg 34%); chlorite can be found in three samples, with its content between 5 and 10% (avg 7%). With the increase in burial depth, the content of kaolinite and illite gradually increases, while the content of I/S decreases (Figure 3). The mixed layer ratio(S%) of I/S decreased from 30% to 10%, indicating the I/S is gradually transformed from disordered to ordered mixed layers.

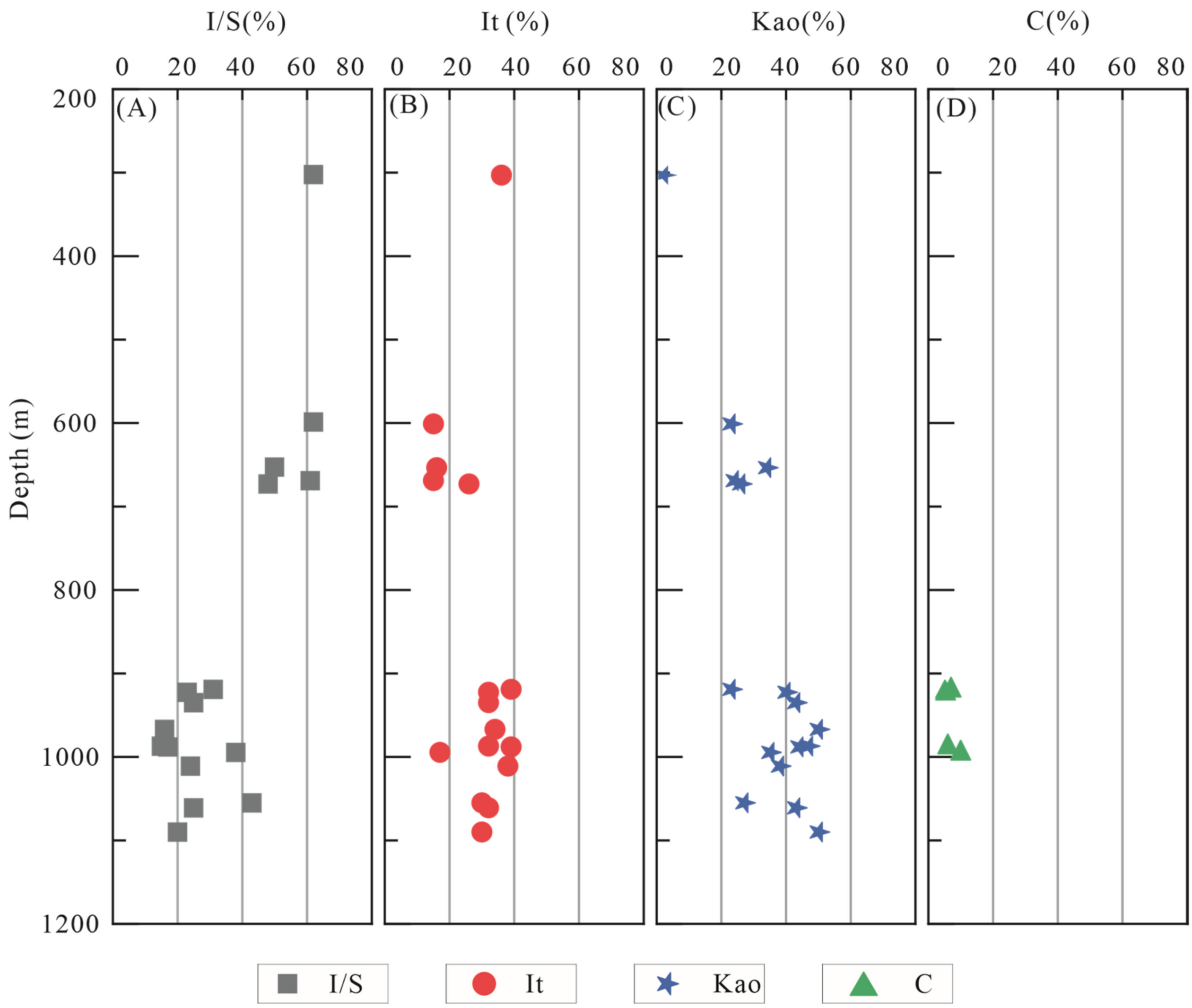

Figure 3. Relative contents of different clay minerals with increasing depth. (**A**) illite/smectite mixed layers; (**B**) illite; (**C**) Kaolinite; (**D**) chlorite.

4.2. Physical Properties of Coal Measure Sandstone

The core porosity of the coal measure sandstone ranges from 1.25 to 10.86% (avg of 3.37%, Figure 2A), and the permeability of the core samples is in the range of 0.00016–0.539 mD (avg on 0.083 mD, Figure 2B) which is mainly composed of lots of low permeability and low porosity sandstone and several tight sandstones. As the depth increases, the porosity and permeability of the sandstone samples decrease accordingly, and the correlation between porosity and depth is more obvious.

4.3. Characterization of Sandstone Storage Space

4.3.1. Pore Structure Characterization

The results of the HPMI test can provide effective parameters for evaluating pore connectivity [15,36,37]. The average pore-throat radius of the coal-bearing sandstones of the Xishanyao formation ranges from 0.010 to 0.616 um, with a mean value of 0.133 um (Table 2); the discharge pressure ranges from 0.26 to 13.79 Mpa; the median pore-throat radius ranges from 0.006 to 0.331 um (Figure 2D); the maximum injected mercury saturation ranges from 34.91% to 96.19%, and the mercury withdrawal efficiency ranges from 25.29% to 73.21 (Table 2). Overall, the sandstone pore-throat radius and the connectivity in this area are moderate. Combined with the analysis of the physical property results, the relationship between the permeability and the median pore-throat radius is better than the relationship between the permeability with mean grain size or porosity (Figure 4A–C), which also indicates that the pore-throat radius is an important factor in determining the seepage capacity [55].

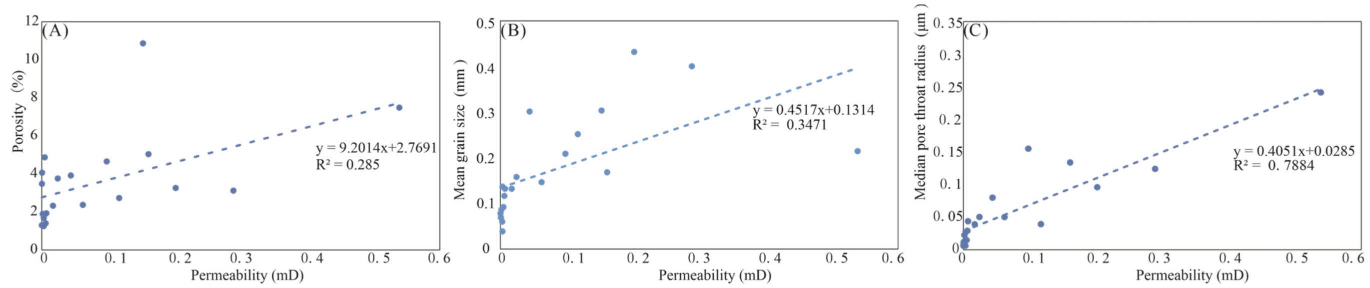

Figure 4. Plots of the relationship between permeability with porosity (**A**), average grain size (**B**), and median pore throat radius (**C**).

Nitrogen adsorption experiments show that the mesopore volume of the Xishanyao formation coal measure sandstone is higher than others, and the adsorption volume is 134×10^{-5}–1348×10^{-5} mL/g (avg on 393×10^{-5} mL/g) followed by the macropore with an adsorption volume of 37×10^{-5}–325×10^{-5} mL/g (avg on 128×10^{-5} mL/g). The micropore adsorption volume is the smallest, which is 23×10^{-5}–244×10^{-5} mL/g (avg on 69×10^{-5} mL/g). The specific surface area is between 0.409 and 6.53 m^2/g, with an average value of 1.77 m^2/g. The origin of pores in different diameters is quite different, which means pore volume distribution can help analyze the influence of diagenesis [56].

4.3.2. Types of Storage Space

The observations from casting thin sections and SEM of the coal measure sandstone of the Xishanyao formation show that the storage space in the study area mainly includes primary pores, secondary pores and fractures. The proportion of primary pores is relatively small, mainly residual primary pores (RIPs), which are triangular or polygonal shapes (Figure 5C,D). The secondary pores are relatively abundant, mainly composed of intergranular dissolved pores (such as carbonate cemented dissolution pores, Figure 5B,C), intragranular dissolved pores (such as feldspar and lithic fragment dissolution pores) (Figure 5A) and a small amount of inter-crystalline pores (kaolinite inter-crystalline pores, dolomite inter-crystalline pores, Figure 5E,F). Among them, the surface of the intergranular dissolved pores is relatively irregular, while the intragranular dissolved pores are mostly located on the surface of the debris particles. The fractures in the sandstone include intragranular fractures and intergranular fractures, which are mostly formed under strong compaction. The existence of these fractures improves reservoir permeability to a certain extent.

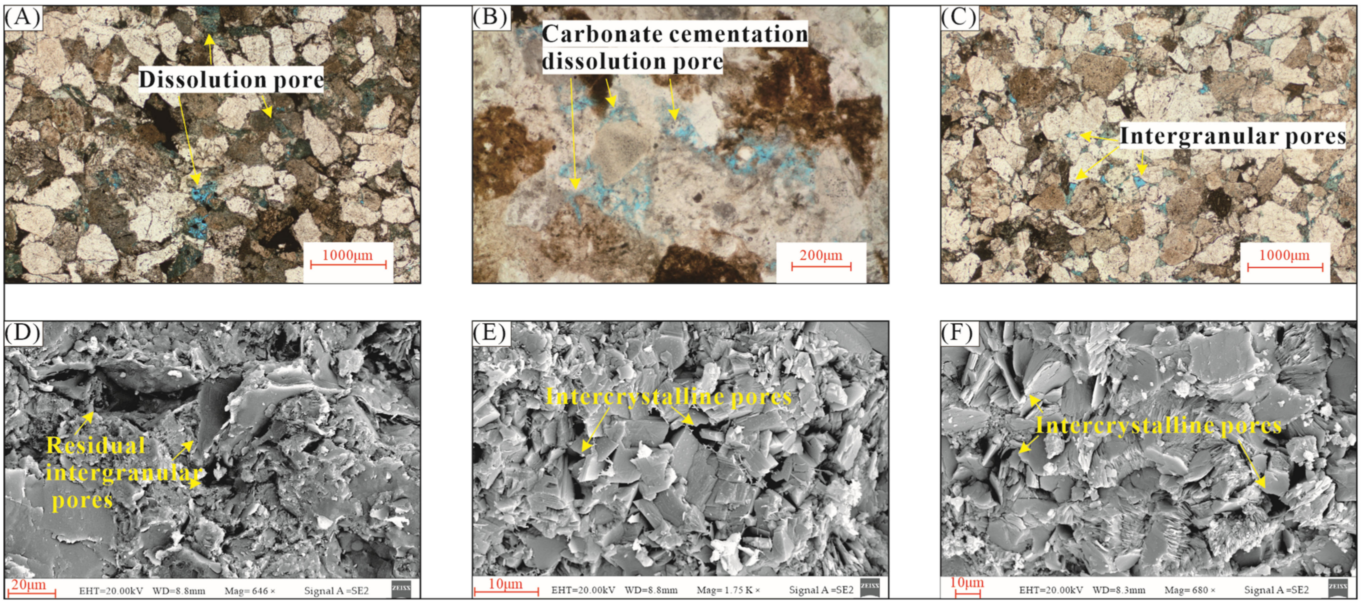

Figure 5. Pore types of coal measure sandstone. (**A**) Intergranular dissolution pores; (**B**) Cementation dissolution pores; (**C**) Intergranular pores; (**D**) Residual intergranular pores; (**E**) Dolomite inter-crystalline pores; (**F**) Kaolinite inter-crystalline pores.

4.4. Diagenesis Feature

4.4.1. Compaction

The constantly increasing weight of the overlying water and sediments results in compaction degree increases, and in the sediments appear a series of phenomena, such as interlayer water discharge, volume reduction, porosity reduction, and permeability decline [29,37,57,58]. Mechanical compaction causes the rearrangement and breaking of the rigid grains and deforms plastic particles, which will reduce the pore space in the reservoir and inhibits cementation and dissolution [25,59]. Further intensification of the pressure leads to the occurrence of chemical compaction, which is characterized by suture contact. The compaction phenomenon observed in coal measure sandstones indicates intense compaction during the diagenetic stage: particle contact types include linear contact (Figure 6A), concave–convex contact (Figure 6A,D) and suture contact (Figure 6F); rigid particles, such as quartz and feldspar are broken to produce cracks (Figure 6A,F–H); feldspar particles are in a semi-oriented arrangement (Figure 6D,F); plastic components, such as mica, plastic lithic fragments, and carbonaceous fragments are bent and deformed (Figure 6D–F).

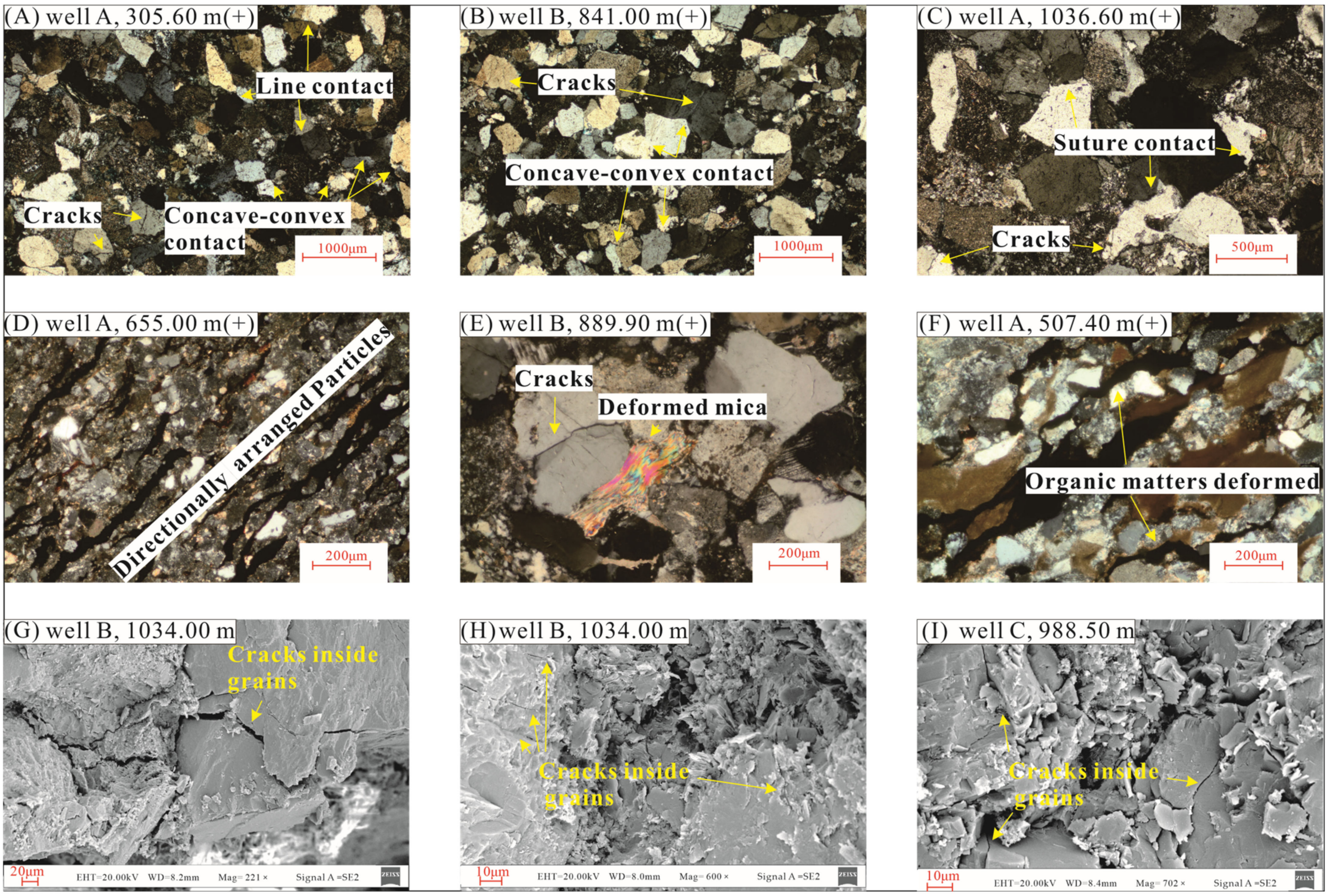

Figure 6. Characteristics of compaction show on casting thin sections and SEM images in the southern margin of Junggar basin. (**A**,**B**) the line contact and the concave–convex contact of the detrital particles, and intragranular fissures can be found on the detrital particles; (**C**) the concave–convex contact and suture contact of detrital particles; (**D**) the compacted plastic particles and semi-directional distributed rigid particle; (**E**) the deformed mica; (**F**) organic debris and boulder clay filled pores and fissures; (**G**–**I**) the intragranular fractures. In the thin section picture, (+) means orthogonally polarized light.

4.4.2. Cementation

- Quartz cement;

Quartz cement commonly occurs in acidic diagenetic environments, usually in the form of overgrowths around detrital quartz grains [13,60], and the fluid inclusions, irregular erosion and remnant clay films often occur in the boundaries of quartz grains and quartz cementation (Figure 5A,C). The quartz grains in the study area are rarely observed to be encrusted with clay films, which makes the overgrowth hard to identify. In eodiagenesis, quartz cementation tends to be associated with I/S mineral transformations, and in the mesodiagenesis stage, the quartz cementation may result from the chemical compaction of quartz grains and the dissolution of feldspar and lithic fragments [5,19,23,61–64].

- Clay mineral cement;

The clay minerals' cementation is the major cementation type in the SJB which usually occurs in the form of authigenic shapes filling the pores or covering the surface of the grains [13,65] (Figure 7D). The authigenic shape of kaolinite is usually booklet and helminthoid filled in intergranular pores and dissolution pores [5] (Figure 7E,G), and its origin is usually associated with the dissolution of feldspar and aluminosilicate lithic fragments [43]. The illite in the SJB is generally in a flaky, fibrous shape and covers the surface of the grains [55] (Figure 7E–I). In addition, illite was also found on the surface of dolomite crystals, which showed the persistence of illite cementation in diagenesis (Figure 7H). The I/S is the product of the smectite/illite transformation, usually in the form of honeycomb-filled pores [65] (Figure 7F).

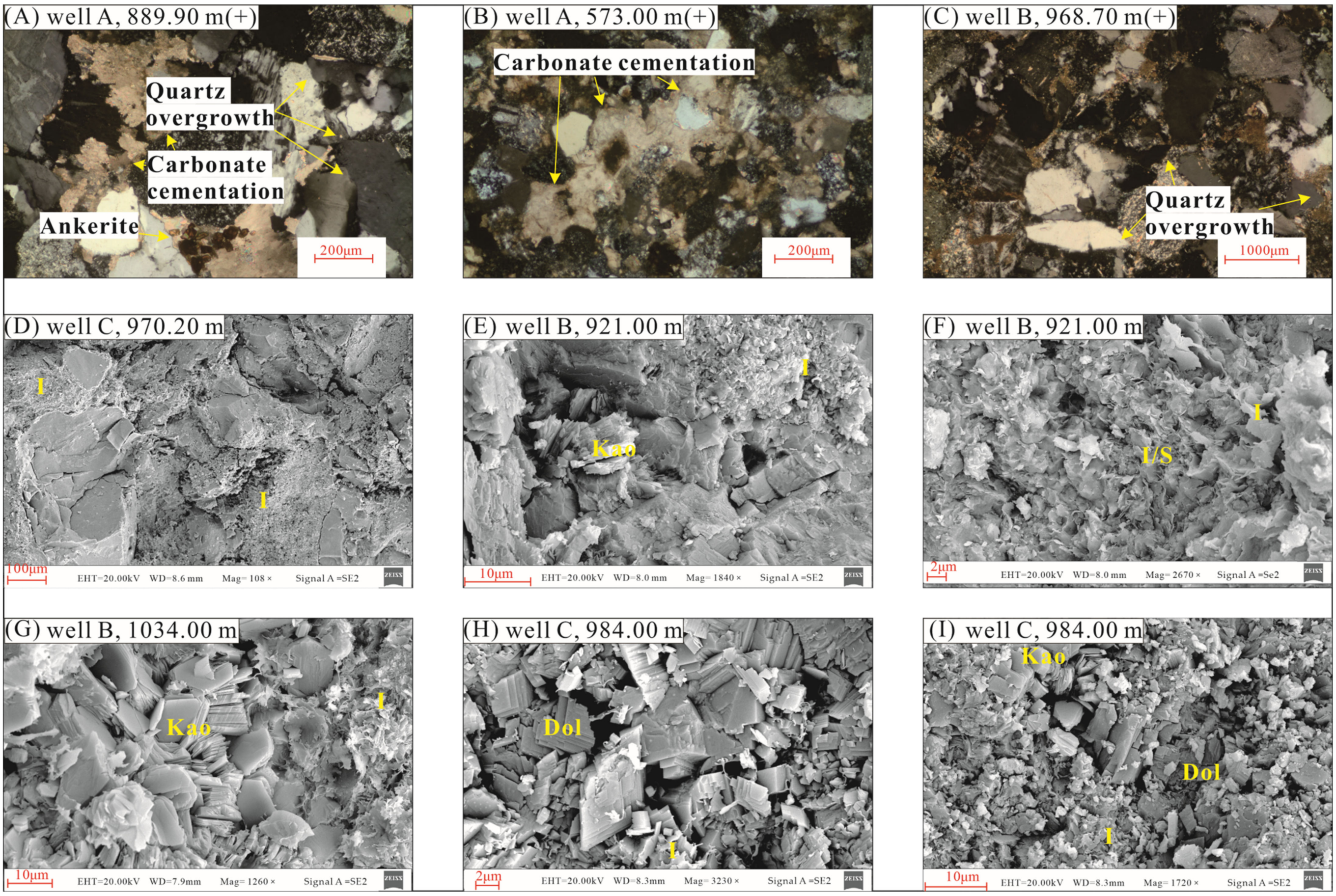

Figure 7. The characteristics of cementation are shown in casting thin sections and SEM images in the study area. (**A**) the cementation of micrite carbonate and dolomite, and the quartz overgrowth; (**B**) micrite carbonate cemented filled intergranular pores; (**C**) quartz overgrowth, clay minerals cement filling pores, and sericitization of volcanic lithic fragments; (**D**) illite cement in close contact with detrital particles; (**E**) kaolinite and illite cement filled pores; (**F**) illite and I/S cement fill intergranular pores; (**G**) the kaolinite inter-crystalline pores; (**H**) dolomite fills intergranular pores and forms inter-crystalline pores, while the illite is attached to the surface dolomite; (**I**) kaolinite and illite and dolomite cement fill the intergranular pores. In the thin section picture, (+) means orthogonally polarized light.

- Carbonate cement;

During the mesodiagenesis A2 stage, the organic acid content was greatly reduced due to high-temperature decomposition and consumption of dissolution, resulting in a gradual weakening of the acidic diagenetic environment. The $CO_3{}^{2-}$ generated from the dissolution of early period carbonate cement and the thermal evolution of organic matter combines with the Ca^{2+}, Fe^{2+} and Mg^{2+} ions that come from the dissolution of early period carbonate cement to form the dolomite and ankerite cement [65]. These late period carbonate cement (dolomite and ankerite) filled the residual intergranular pores (Figure 7A,B,H,I).

4.4.3. Dissolution

The coal measure sandstones of the Xishanyao formation have been strongly modified by dissolution due to the large amounts of organic acids released during the thermal evolution of the coal measure source rock (mainly from coal seams and some from dark shales). The dissolution occurs mainly in feldspars, Equations (1)–(3), lithic fragments (Figure 8A,B,E,F), and carbonate cement (Figure 8C,D). Compared with the dissolution of feldspar, the dissolution of carbonate cement is often accompanied by a lower chemical equilibrium constant, thus requiring a lower PH value of the diagenetic environment [41,66]. There are numerous particle dissolutions pores (Figure 8A,B,G–I), casting pores (Figure 8A,B,E,F) and intergranular pores produced by cement dissolution (Figure 8C,D) in the casting thin sections and SEM image.

$$2KAlSi_3O_8 + 2H^+ + H_2O = Al_2Si_2O_5(OH)_4 + 4SiO_2 + 2K^+, \quad (1)$$

$$2NaAlSi_3O_8 + 2H^+ + H_2O = Al_2Si_2O_5(OH)_4 + 4SiO_2 + 2Na^+, \quad (2)$$

$$CaAl_2Si_2O_8 + 2H^+ + H_2O = Al_2Si_2O_5(OH)_4 + Ca^{2+} + 3Al^{3+}, \quad (3)$$

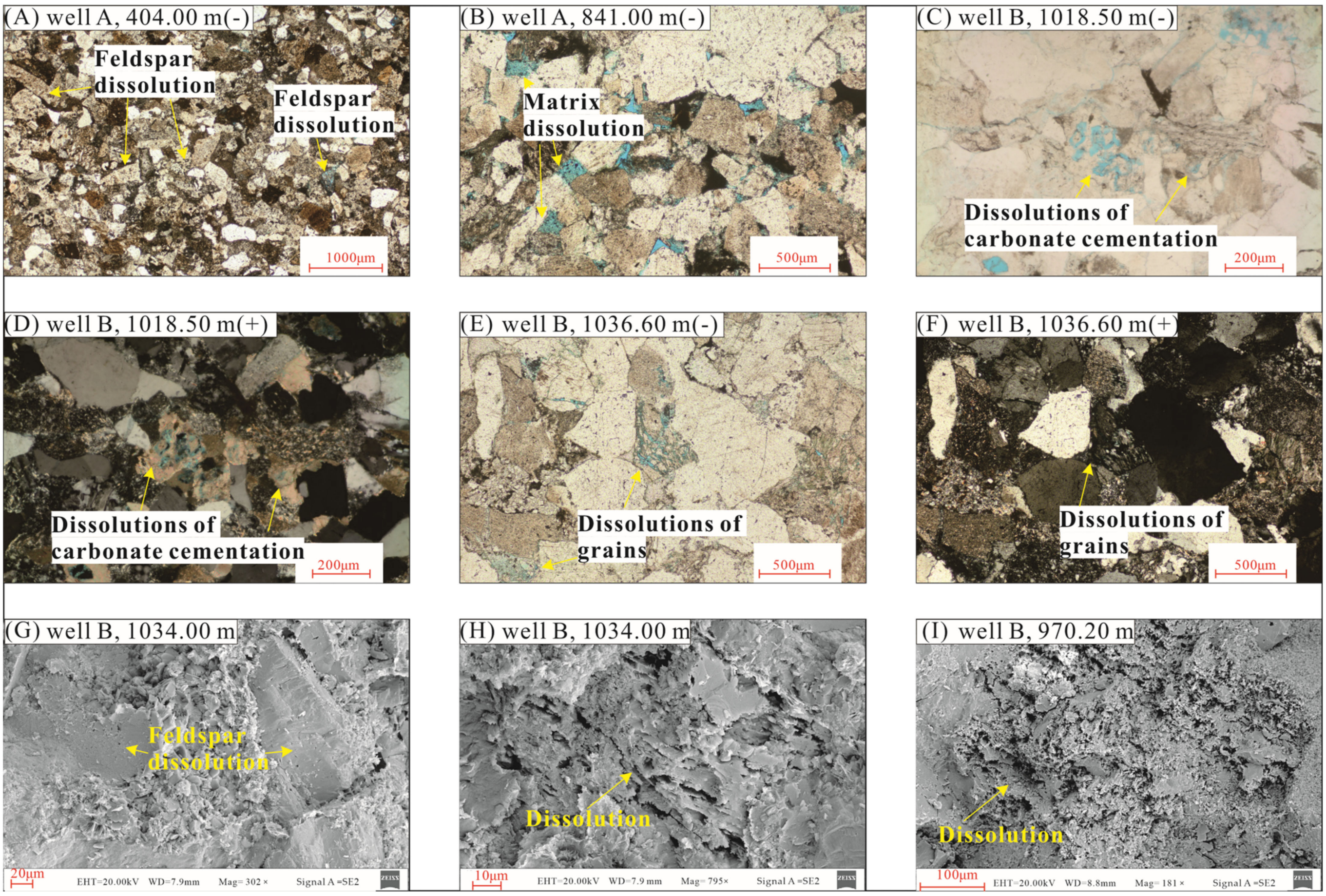

Figure 8. Characteristics of dissolution show on casting thin sections and SEM images in the study area. (**A**) dissolution of feldspar and volcanic lithic fragments. (**B**) dissolution of feldspar, lithic fragments and matrix; (**C**,**D**) the dissolution pores that are formed by dissolution of micrite carbonate cementation; (**E**,**F**) feldspar dissolves along the cleavage plane, forming dissolution pores and fractures; (**G**) dissolution on feldspar particle surface with the kaolinite filling the intergranular pores; (**H**,**I**) directional dissolution of feldspar particle. In the thin section picture, (+) means orthogonally polarized light and (-) means plane polarized light.

5. Discussion

5.1. Paragenetic Sequence of Coal Measure Sandstone Diagenesis

5.1.1. Determination of Diagenetic Stage

The clarification of diagenetic stages should be based on paleo-temperature (T), vitrinite reflectance (Ro), maximum pyrolysis peak temperature (Tmax), and smectite mixed layer ratio (S%) of I/S, spatial and temporal assemblages of authigenic minerals and the contact relationships between particles [5,22,67]. The Ro of coal measure shale in the Xishanyao formation in the study area ranges from 0.63–0.89%. The clay minerals of the coal measure sandstone are dominated by I/S, kaolinite and illite, with the mixed layer ratio (S%) of I/S ranging from 10–30% (avg on 18%). The compaction strongly influences the coal measure sandstone, with contact relationships composed of line contact, concave–convex contact, and suture contact. The reconstructed thermal history of the Jurassic strata, which is conducted by Wang et al. [68], found that the maximum burial depth of the Xishanyao formation exceeded 3000 m and the paleotemperature exceeded 100 °C. According to the diagenetic stage classification standard of clastic rocks (China's oil and gas industry standard SY/T5477-2003), it can be comprehensively determined that the diagenetic stage of the Xishanyao formation coal measure sandstone is in the mesodiagenesis A1 and A2 stage (Figure 8).

5.1.2. Diagenetic Sequences of Coal Measure Sandstone

Combining with the thermal and burial history of the SJB, referring to the division of diagenetic stages in clastic rocks of China's oil and gas industry standard SY/T5477-2003, the diagenetic evolution of the Xishanyao formation coal measure sandstone in the area is summarized as follows:

- Syndiagenesis

In this stage, the diagenetic environment has not been completely disconnected from the overlying water. The organic matter deposited in the peat swamp generates CO_2 under the action of microorganisms and dissolves in water, making the diagenetic environment weakly acidic. Due to the acidic nature of the sedimentary water, the surface of the detrital particles is rarely coated by a chlorite clay film. Due to the strong hydrodynamic environment during the sedimentary period, the coal measure sandstone contains a certain amount of plastic micrite carbonate and carbonaceous fragments will be blended into the sandstone.

- Eodiagenesis (at the depth < 2 km, temperature < 70 °C, and Ro < 0.5%)

The type and degree of diagenesis in the eodiagenesis stage will affect the type of diagenesis and the physical properties of the reservoir in the later diagenetic stage [22]. At this stage, the diagenetic environment is weakly acidic, and the diagenesis types include mechanical compaction, cementation (mainly argillaceous cementation) and dissolution, and the diagenetic environment gradually changes to a closed system. The compaction significantly reduces primary porosity [69,70], due to the shallow burial depth and the high subsidence rate. The rock is in a weakly consolidated and semi-consolidated state, and the contact relationships of the clastic particles change from point contact to point-line contact. Pore types of the coal measure sandstone in this stage are mainly primary pores, and a small amount of micrite carbonate cement fills the pores.

With the increase in temperature, the coal seams and dark shale gradually released organic acid and CO_2 [64], which makes the diagenetic environment gradually change to a weak acid. The feldspar and detrital grains began to dissolve slightly and form dissolution pores (Figure 9).

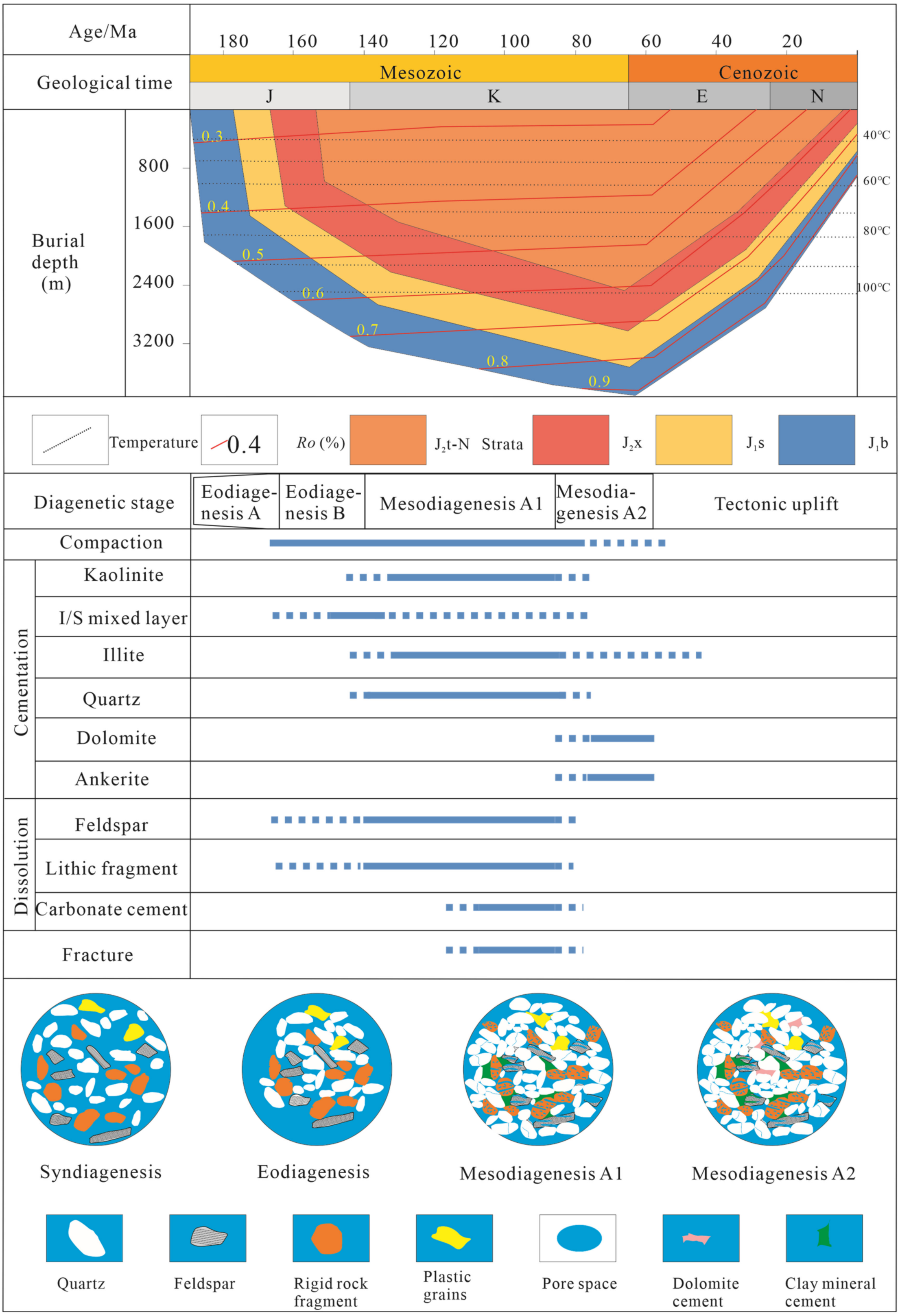

Figure 9. The paragenetic sequence and pore evolution of the Xishanyao formation in the SJB. The thermal evolution history is based on the study of Wang et al. [68] with some modifications. Solid blue lines represent probable timing based on observed diagenetic and mineralization phases. While the dashed blue lines represent inferred or not well-constrained diagenetic and mineralization phases. J_2x = Xishanyao formation; I/S = illite/smectite; Ro = vitrinite reflectance.

- Mesodiagenesis (at the depth > 2 km, temperature > 70 °C, and Ro > 0.5%)

The effect of compaction in the mesodiagenesis A stage was extremely strong, and the compaction type gradually shifted from mechanical compaction to chemical compaction. The contact relationships change from point contact and line contact to line contact, concave–convex contact and suture contact during this stage, along with a large proportion of brittle minerals broken up. The dissolution pores formed in the eodiagenesis stage are damaged under the compaction, and the damage of compaction to the quality of the reservoir is further strengthened. The mesodiagenesis A stage can be further divided into two substages, A1 and A2, according to temperature and Ro. These two substages have certain differences in diagenetic environment and diagenetic reaction:

In the mesodiagenesis A1 stage, the temperature was 70–90 °C, and the Ro was 0.5–0.7%, in an acidic diagenetic environment. The amount of organic acid generated in coal measures reaches the highest level at this temperature [71], the diagenetic environment is acidic, and the tensity of dissolution reached the highest level (Figure 9). The massive dissolution of feldspar, aluminosilicate lithic fragments and early micrite carbonate cement formed a large number of dissolution pores and mold pores. Because of the relatively closed diagenetic system, the dissolution products cannot be discharged. This has led to the kaolinite filling pores and quartz overgrowth (part of the SiO_2 comes from the chemical compaction).

In the Mesodiagenesis A2 stage, the temperature was 90–130 °C, and the Ro was 0.7–1.3%. The acidic diagenetic environment is gradually weakened due to the decomposition of organic acids. The effect of dissolution decreases gradually, while the cementation is gradually increases. The quartz overgrowth gradually decreases, which is manifested as second level quartz cementation. Late period carbonate cementation (dolomite and ankerite) gradually filled the pore space (Figure 9). The clay minerals appear abundantly and fill the pores, further reducing the porosity.

5.2. Diagenetic Control of Coal Measure Rvoir Quality

Reservoir quality is influenced by diagenetic activities, such as compaction, cementation, dissolution, recrystallization, and metasomatism [20,72]. For the Xishanyao formation coal measure sandstone, compaction, dissolution and cementation are the main diagenetic controlling factors for reservoir quality.

5.2.1. The Influence of Compaction on Reservoir Quality

The compaction is one of the main factors that cause the reduction of intergranular pore volume [73] and the densification of coal measure sandstone reservoirs. Plastic particles in the sandstone have a weak compaction resistance, while the rigid particles have a high compaction resistance ability [61,74]. The coal measure sandstones of the Xishanyao formation contain a high content of plastic grains, such as volcanic lithic fragments, muddy gravel and carbonaceous fragments, which makes its compaction resistance ability weak.

The coal measure sandstone reservoirs are strongly affected by mechanical compaction, which is characteristic of the close contacted clastic particles, the ruptured rigid particles, and the deformed plastic particles. Chemical compaction commonly happens in SJB due to the high intensity of compaction, which may lead to particle suture contact and reduced interparticle space. The intense mechanical and chemical compaction has a great negative effect on the physical properties of the sandstone reservoir.

5.2.2. The Influence of Cementation on Reservoir Quality

The coal measure sandstone of the Xishanyao formation in the SJB is mainly clay mineral cement, followed by quartz cement and carbonate cement. The development of these cementations is one of the main factors leading to the significant decline in reservoir quality [74–77].

The closed diagenetic system of coal measure sandstone prevents the dissolution products from being discharged in time, which also leads to the development of authigenic kaolinite cementation and quartz cementation. The developed kaolinite cement fills the pore space in large quantities, but its loose inter-crystalline structure contains inter-crystalline pores that can resist compaction [78]. In addition, illite and I/S mainly fill intergranular pores and pore throats, thereby reducing the reservoir quality of the sandstone [65,79,80]. In summary, different types of clay minerals occur widely and fill or divide the pore space, resulting in tortuous pore throats, reducing pore connectivity, and weakening seepage capacity [13,37,65,79,80].

The content of volcanic lithic fragments in coal measure sandstone is relatively high, which may inhibit the quartz overgrowth to some extent [77]. It can be observed that the overgrowth level of the coal measure sandstone is shown in the second stage (Figure 5A,C). The quartz overgrowth in the eodiagenesis stage can help the sandstone better resist compaction. In the mesodiagenesis, pressure solution, feldspar dissolution and clay mineral transformation produced many SiO_2 (aq), which developed into the quartz cement [13,81,82].

The carbonate cement is locally developed in coal measure sandstones. In the eodiagenesis stage, several micrite carbonate particles blended in the coal measure sandstone, which blocked and filled the intergranular pores. In the mesodiagenesis A2 stage, the late period dolomite and ankerite cements appeared in the sandstone, which blocked the intergranular pores of the sandstone and reduced the reservoir quality (Figure 5A,H,I).

5.2.3. The Influence of Dissolution on Reservoir Quality

The dissolution in diagenesis has a positive effect on reservoir physical properties [13]. The coal seam and dark shale begin to produce organic acids through the decomposition of plant residues during the eodiagenesis stage [71] and reaching a peak in the mesodiagenesis stage (temperature range from 80 °C to 140 °C, [37,83]). The amount of organic acid generated in the coal measure is much higher than in other source rocks [5,7,84].

The sedimentary environment makes the sandstone have good primary physical properties and pore connectivity, and the weak dissolution in the eodiagenesis stage provides a seepage channel for the migration of acidic fluids in the mesodiagenesis stage. The large proportion of aluminosilicate minerals, such as feldspar and volcanic in coal measure sandstone provides a good material basis for the dissolution [5]. Dissolution is most intense in mesodiagenesis. During this period, the thermal evolution of organic matter releases a large number of organic acids into the diagenetic system of the sandstone, causing the soluble minerals to selectively dissolve and form a large number of intragranular dissolved pores and intergranular dissolution pores [35]. Overall, the diagenetic stage of the coal measure sandstone in this area is mainly in the A1 and A2 stages of the mesodiagenesis, which happens to be the most intense stage of organic acid dissolution. The dissolution has brought a great positive effect on the physical properties of the reservoir.

5.2.4. The Origin of Authigenic Clay Minerals in Coal Measure Sandstone

Clay mineral cement has a great influence on the physical properties of coal measure sandstone reservoirs. The coal measure sandstone has a high content of kaolinite (2–50%, avg 34%) and some chlorite (5–10% in 4 samples) which is abnormal in coal measure. The discussion of their origins could offer more information to help us understand the diagenetic characteristic of coal measure sandstone.

The origin of kaolinite in authigenic minerals mainly includes (1) weathering of medium-acid magmatic rocks and metamorphic rocks during sedimentation [85]; (2) dissolution of volcanic lithic fragments and feldspar during diagenesis, Equations (1)–(3) [13]; (3) the alternation of unstable illite into stable kaolinite in an acidic environment [5]. Based on the evidence of relatively strong dissolution in the sandstone, the high content of volcanic lithic fragment and feldspar and the developed authigenic quartz in sandstone, it can be considered that the kaolinite in the study area mainly comes from the dissolution.

The formation of chlorite requires Fe^{2+} and Mg^{2+}. Based on the source of Fe^{2+} and Mg^{2+}, the formation of chlorite mainly includes (1) direct precipitation in the delta sedimentary environment due to the difference in electrolytes between rivers and lakes during sedimentation [86,87]; (2) formed by the transformation of smectite under an alkaline environment, and this process is marked by the existence of chlorite/smectite mixed layers [87]; (3) the interaction of feldspar and Fe^{2+} and Mg^{2+} generated by the dissolution of volcanic lithic fragments Equation (4) [86–88]. However, no chlorite clay film was found during the thin section observation, and no chlorite/smectite mixed layer was detected in the whole-rock and clay mineral analyses result (Table 1), which means the chlorite in the study area did not originate from the first two reasons. Considering the strong dissolution in the study area while the sandstone containing chlorite is in the mesodiagenesis A2 stage, it can be interpreted that the chlorite in the study area is mainly formed by the interaction of feldspar and Fe^{2+} and Mg^{2+} formed by the dissolution of volcanic lithic fragments Equation (4).

$$\underset{\text{(K-feldspar)}}{2KAlSi_3O_8} + 0.4Fe^{2+} + 0.3Mg^{2+} + 1.4H_2O = \underset{\text{(chlorite)}}{0.3(Fe_{14}Mg_{12}Al_{2.5})(Al_{0.7}Si_{3.3})O_{10}(OH)_8} + 2SiO_2 + 0.4H^+ + K^+ \quad (4)$$

5.3. The Influence of Sedimentation on the Reservoir Quality of Coal Measure Sandstone

The influence of the sedimentation on reservoir quality cannot be well evaluated only by sedimentary facies, which need to be analyzed from the aspects of composition, texture, and diagenetic alteration [19,72,89–91].

The parameters, such as the average particle size, sorting, roundness, and matrix content of the sandstone determine the initial intergranular volume [15,21,32,92,93], and the initial porosity of sediment can reach 40% [94]. Permeability is a function of the matrix and grain size [39,95]. For sandstones in the same diagenetic stage, the larger the average grain size, the better the sorting and roundness; the lower the matrix content, the stronger the compaction resistance, and the better the physical properties of the reservoir will be [96,97]. Reservoirs with good physical properties are conducive to the exchange of fluids, thereby enhancing the strength of cementation and dissolution during diagenesis [67,98].

The coal measures sandstone in the Xishanyao formation is formed in a lacustrine-braided river delta environment [1,3]. The sandstone particles are poor to medium sorted, sub-angular to sub-round roundness, have high matrix content, and have a medium-high texture maturity. Coal measure sandstones with medium-high texture maturity are prone to grain rearrangement (rotation and slippage) during compaction, thereby enhancing the effect of compaction [99].

Differences in the composition of particles lead to differences in physical and chemical diagenesis reactions during diagenesis [67,98,100]. When the quartz content is low, the reservoir quality increases with the increase in the quartz content. If the content of detrital quartz is higher than 75%, the lower content of feldspar will lead to the reduction of dissolved pores, and at the same time, the quartz cementation in the reservoir will be more developed, thereby reducing the porosity and permeability of the reservoir [101,102].

The compositional maturity of coal measure sandstone in the SJB is relatively low, and its provenance is composed of pyroclastic rocks, intermediate-acid magmatic rocks, and metamorphic rocks derived from the Tianshan Mountains [46,54]. Because the provenance is closer to the depositional area, the proportion of feldspar and volcanic lithic fragments in the coal measure sandstone is relatively large. Due to the weak compaction resistance of feldspar, lithic fragments and plastic particles (such as muddy gravel and carbonaceous fragments) [103,104], the coal measure sandstone reservoirs are greatly affected by mechanical compaction. In addition, the abundant organic matter and the high content of feldspar and lithic fragments in the coal measure strata also lead to strong dissolution during the diagenetic stage.

Due to the warm and humid environment during the deposition period of the Xishanyao formation, the coal measures are generally developed. The abundant organic matter generated CO_2 under the action of microbial fermentation and made the water weakly acidic [9]. The weakly acidic water medium condition makes it difficult to coat clay minerals on the grain surface and form chlorite clay films. The absence of the clay film on the grain surface makes the reservoir easily affected by compaction and makes the observation of quartz overgrowth more difficult. In addition to the dissolution during the diagenesis, a part of kaolinite is also formed during the depositional period, and their origins were mainly because of the mineral transformation, illite and chlorite under acidic conditions, and feldspar alteration [5,65,85].

6. Conclusions

The petrological and mineralogical results of the coal measure sandstone samples of the Xishanyao formation in the southern margin of the Junggar basin show that:

1. Coal measure sandstone reservoirs are characterized by a high content of quartz, feldspar and clay minerals, poor to moderate sorting, sub-angular to sub-round roundness, and generally high matrix content. The porosity and permeability of the sandstone layers are low, and multiple samples can be categorized as tight sandstone.

2. The coal measure sandstone is in the mesodiagenesis A1-A2 stage. The effect of compaction in the eodiagenesis was significant, accompanied by a small amount of feldspar and lithic fragments dissolution, kaolinite and illite precipitation, I/S transformation, and quartz cementation. In the mesodiagenesis stage, the influence of compaction is relatively reduced while the I/S transformation level is increased. In the mesodiagenesis A1 stage, the dissolution strength reached the highest level, and the clay mineral and quartz cement were also intense. In the mesodiagenesis A2 stage, the dissolution strength gradually weakened when the late period carbonate cement appeared.

3. The compaction, cementation and dissolution are the three diagenetic factors that control the reservoir quality of the coal measure sandstone. Among them, compaction is the main factor that makes the reservoir quality decline. Dissolution produces massive dissolved pores, which improves the quality of the reservoir significantly. The kaolinite and quartz cementation formed by the precipitation of undischarged dissolution products block the pores and pore throats and deteriorate the reservoir quality.

4. The sedimentary environment influences the texture, composition and diagenetic alteration of coal measure sandstone. The medium-good texture maturity and a large content of volcanic lithic fragments and feldspar of the coal measure sandstone make it susceptible to the influence of compaction and dissolution.

Author Contributions: Conceptualization, D.T. and S.C.; methodology, S.T. and S.C.; software, A.Z., Y.P. and T.Z.; validation, A.Z., Y.P. and D.T.; formal analysis, A.Z.; investigation, A.Z., Y.P., B.S. and T.Z.; resources, D.T.; data curation, A.Z.; writing—original draft preparation, A.Z.; writing—review and editing, A.Z., S.C. and S.T.; visualization, A.Z. and S.T.; supervision, D.T. and S.T.; project administration, D.T. and S.C.; funding acquisition, D.T. and B.S. All authors have read and agreed to the published version of the manuscript.

Funding: The research was financially supported by the National Natural Science Foundation of China (Grant No. 42102205), and the PetroChina Company Limited "14th Five Year Plan" Science and Technology Major Project (Grant No. 2021DJ2306).

Data Availability Statement: Not applicable.

Acknowledgments: We would like to thank the Xinjiang Coalfield Geology Bureau and the No. 156 Coalfield Geological Exploration Team of the Xinjiang Coalfield Geology Bureau for providing access to convenient field work and core samples.

Conflicts of Interest: The authors declare no conflict of interest.

References

1. Tang, D.; Yang, S.; Tang, S.; Tao, S.; Chen, S.; Zhang, A.; Pu, Y.; Zhang, T. Advance on Exploration—Development and Geological Research of Coalbed Methane in the Junggar Basin. *J. China Coal Soc.* **2021**, *46*, 2412–2425. [CrossRef]
2. Li, Y.; Shao, L.; Hou, H.; Tang, Y.; Yuan, Y.; Zhang, J.; Shang, X.; Lu, J. Sequence Stratigraphy, Palaeogeography, and Coal Accumulation of the Fluvio-Lacustrine Middle Jurassic Xishanyao Formation in Central Segment of Southern Junggar Basin, NW China. *Int. J. Coal Geol.* **2018**, *192*, 14–38. [CrossRef]

3. Fu, H.; Tang, D.; Xu, H.; Xu, T.; Chen, B.; Hu, P.; Yin, Z.; Wu, P.; He, G. Geological Characteristics and CBM Exploration Potential Evaluation: A Case Study in the Middle of the Southern Junggar Basin, NW China. *J. Nat. Gas. Sci. Eng.* **2016**, *30*, 557–570. [CrossRef]
4. Fu, H.; Tang, D.; Pan, Z.; Yan, D.; Yang, S.; Zhuang, X.; Li, G.; Chen, X.; Wang, G. A Study of Hydrogeology and Its Effect on Coalbed Methane Enrichment in the Southern Junggar Basin, China. *Bulletin* **2019**, *103*, 189–213. [CrossRef]
5. Li, Y.; Gao, X.; Meng, S.; Wu, P.; Niu, X.; Qiao, P.; Elsworth, D. Diagenetic Sequences of Continuously Deposited Tight Sandstones in Various Environments: A Case Study from Upper Paleozoic Sandstones in the Linxing Area, Eastern Ordos Basin, China. *Bulletin* **2019**, *103*, 2757–2783. [CrossRef]
6. Li, Y.; Yang, J.; Pan, Z.; Meng, S.; Wang, K.; Niu, X. Unconventional Natural Gas Accumulations in Stacked Deposits: A Discussion of Upper Paleozoic Coal-Bearing Strata in the East Margin of the Ordos Basin, China. *Acta Geol. Sin. Engl. Ed.* **2019**, *93*, 111–129. [CrossRef]
7. Qin, Y. Research Progress of Symbiotic Accumulation of Coal Measure Gas in China. *Nat. Gas Ind. B* **2018**, *5*, 466–474. [CrossRef]
8. Zou, C.; Yang, Z.; Huang, S.; Ma, F.; Sun, Q.; Li, F.; Pan, S.; Tian, W. Resource Types, Formation, Distribution and Prospects of Coal-Measure Gas. *Pet. Explor. Dev.* **2019**, *46*, 451–462. [CrossRef]
9. Fu, H.; Li, Y.; Su, X.; Yan, D.; Yang, S.; Wang, G.; Wang, X.; Zhao, W. Environmental Conditions and Mechanisms Restricting Microbial Methanogenesis in the Miquan Region of the Southern Junggar Basin, NW China. *GSA Bull.* **2022**. [CrossRef]
10. Li, Y.; Fu, H.; Yan, D.; Su, X.; Wang, X.; Zhao, W.; Wang, H.; Wang, G. Effects of Simulated Surface Freshwater Environment on in Situ Microorganisms and Their Methanogenesis after Tectonic Uplift of a Deep Coal Seam. *Int. J. Coal Geol.* **2022**, *257*, 104014. [CrossRef]
11. Zhang, L.; Bai, G.; Luo, X.; Ma, X.; Chen, M.; Wu, M.; Yang, W. Diagenetic History of Tight Sandstones and Gas Entrapment in the Yulin Gas Field in the Central Area of the Ordos Basin, China. *Mar. Pet. Geol.* **2009**, *26*, 974–989. [CrossRef]
12. Zou, C.; Zhang, G.; Yang, Z.; Tao, S.; Hou, L.; Zhu, R.; Yuan, X.; Ran, Q.; Li, D.; Wang, Z. Concepts, Characteristics, Potential and Technology of Unconventional Hydrocarbons: On Unconventional Petroleum Geology. *Pet. Explor. Dev.* **2013**, *40*, 413–428. [CrossRef]
13. Yuan, G.; Cao, Y.; Gluyas, J.; Li, X.; Xi, K.; Wang, Y.; Jia, Z.; Sun, P.; Oxtoby, N.H. Feldspar Dissolution, Authigenic Clays, and Quartz Cements in Open and Closed Sandstone Geochemical Systems during Diagenesis: Typical Examples from Two Sags in Bohai Bay Basin, East China. *AAPG Bull.* **2015**, *99*, 2121–2154. [CrossRef]
14. Dutton, S.P.; Loucks, R.G. Reprint of: Diagenetic Controls on Evolution of Porosity and Permeability in Lower Tertiary Wilcox Sandstones from Shallow to Ultradeep (200–6700 m) Burial, Gulf of Mexico Basin, U.S.A. *Mar. Pet. Geol.* **2010**, *27*, 1775–1787. [CrossRef]
15. Lai, J.; Wang, G.; Cai, C.; Fan, Z.; Wang, S.; Chen, J.; Luo, G. Diagenesis and Reservoir Quality in Tight Gas Sandstones: The Fourth Member of the Upper Triassic Xujiahe Formation, Central Sichuan Basin, Southwest China. *Geol. J.* **2018**, *53*, 629–646. [CrossRef]
16. Karim, A.; Pe-Piper, G.; Piper, D.J.W. Controls on Diagenesis of Lower Cretaceous Reservoir Sandstones in the Western Sable Subbasin, Offshore Nova Scotia. *Sediment. Geol.* **2010**, *224*, 65–83. [CrossRef]
17. Wolela, A. Diagenetic Evolution and Reservoir Potential of the Barremian–Cenomanian Debre Libanose Sandstone, Blue Nile (Abay) Basin, Ethiopia. *Cretac. Res.* **2012**, *36*, 83–95. [CrossRef]
18. Zhang, Y.; Pe-Piper, G.; Piper, D.J.W. How Sandstone Porosity and Permeability Vary with Diagenetic Minerals in the Scotian Basin, Offshore Eastern Canada: Implications for Reservoir Quality. *Mar. Pet. Geol.* **2015**, *63*, 28–45. [CrossRef]
19. Taylor, T.R.; Giles, M.R.; Hathon, L.A.; Diggs, T.N.; Braunsdorf, N.R.; Birbiglia, G.V.; Kittridge, M.G.; Macaulay, C.I.; Espejo, I.S. Sandstone Diagenesis and Reservoir Quality Prediction: Models, Myths, and Reality. *AAPG Bull.* **2010**, *94*, 1093–1132. [CrossRef]
20. Bjørlykke, K.; Jahren, J. Open or Closed Geochemical Systems during Diagenesis in Sedimentary Basins: Constraints on Mass Transfer during Diagenesis and the Prediction of Porosity in Sandstone and Carbonate Reservoirs. *AAPG Bull.* **2012**, *96*, 2193–2214. [CrossRef]
21. Morad, S.; Ketzer, J.M.; De Ros, L.F. Spatial and Temporal Distribution of Diagenetic Alterations in Siliciclastic Rocks: Implications for Mass Transfer in Sedimentary Basins. *Sedimentology* **2000**, *47*, 95–120. [CrossRef]
22. El-ghali, M.A.K.; Mansurbeg, H.; Morad, S.; Al-Aasm, I.; Ajdanlisky, G. Distribution of Diagenetic Alterations in Fluvial and Paralic Deposits within Sequence Stratigraphic Framework: Evidence from the Petrohan Terrigenous Group and the Svidol Formation, Lower Triassic, NW Bulgaria. *Sediment. Geol.* **2006**, *190*, 299–321. [CrossRef]
23. Saïag, J.; Brigaud, B.; Portier, É.; Desaubliaux, G.; Bucherie, A.; Miska, S.; Pagel, M. Sedimentological Control on the Diagenesis and Reservoir Quality of Tidal Sandstones of the Upper Cape Hay Formation (Permian, Bonaparte Basin, Australia). *Mar. Pet. Geol.* **2016**, *77*, 597–624. [CrossRef]
24. Burley, S.D.; Kantorowicz, J.D.; Waugh, B. Clastic Diagenesis. *Geol. Soc. Lond. Spec. Publ.* **1985**, *18*, 189–226. [CrossRef]
25. Morad, S.; Al-Ramadan, K.; Ketzer, J.M.; De Ros, L.F. The Impact of Diagenesis on the Heterogeneity of Sandstone Reservoirs: A Review of the Role of Depositional Facies and Sequence Stratigraphy. *AAPG Bull.* **2010**, *94*, 1267–1309. [CrossRef]
26. Yang, S.; Wang, Y.; Zhang, S.; Wang, Y.; Zhang, Y.; Zhao, Y. Controls on Reservoirs Quality of the Upper Jurassic Mengyin Formation Sandstones in Dongying Depression, Bohai Bay Basin, Eastern China. *Energies* **2020**, *13*, 646. [CrossRef]
27. Dashti, R.; Rahimpour-Bonab, H.; Zeinali, M. Fracture and Mechanical Stratigraphy in Naturally Fractured Carbonate Reservoirs-A Case Study from Zagros Region. *Mar. Pet. Geol.* **2018**, *97*, 466–479. [CrossRef]

28. Desbois, G.; Urai, J.L.; Kukla, P.A.; Konstanty, J.; Baerle, C. High-Resolution 3D Fabric and Porosity Model in a Tight Gas Sandstone Reservoir:A New Approach to Investigate Microstructures from Mm- to Nm-Scale Combining Argon Beam Cross-Sectioning and SEM Imaging. *J. Pet. Sci. Eng.* **2011**, *78*, 243–257. [CrossRef]
29. Fisher, Q.J.; Haneef, J.; Grattoni, C.A.; Allshorn, S.; Lorinczi, P. Permeability of Fault Rocks in Siliciclastic Reservoirs: Recent Advances. *Mar. Pet. Geol.* **2018**, *91*, 29–42. [CrossRef]
30. Sakhaee-Pour, A.; Bryant, S.L. Effect of Pore Structure on the Producibility of Tight-Gas Sandstones. *AAPG Bull.* **2014**, *98*, 663–694. [CrossRef]
31. Xiao, L.; Zou, C.; Mao, Z.; Jin, Y.; Shi, Y.; Guo, H.; Li, G. An Empirical Approach of Evaluating Tight Sandstone Reservoir Pore Structure in the Absence of NMR Logs. *J. Pet. Sci. Eng.* **2016**, *137*, 227–239. [CrossRef]
32. Yue, D.; Wu, S.; Xu, Z.; Xiong, L.; Chen, D.; Ji, Y.; Zhou, Y. Reservoir Quality, Natural Fractures, and Gas Productivity of Upper Triassic Xujiahe Tight Gas Sandstones in Western Sichuan Basin, China. *Mar. Pet. Geol.* **2018**, *89*, 370–386. [CrossRef]
33. Stroker, T.M.; Harris, N.B.; Elliott, W.C.; Marion Wampler, J. Diagenesis of a Tight Gas Sand Reservoir: Upper Cretaceous Mesaverde Group, Piceance Basin, Colorado. *Mar. Pet. Geol.* **2013**, *40*, 48–68. [CrossRef]
34. Walderhaug, O.; Eliassen, A.; Aase, N.E. Prediction of Permeability in Quartz-Rich Sandstones: Examples from the Norwegian Continental Shelf and the Fontainebleau Sandstone. *J. Sediment. Res.* **2012**, *82*, 899–912. [CrossRef]
35. Li, P.; Zheng, M.; Bi, H.; Wu, S.; Wang, X. Pore Throat Structure and Fractal Characteristics of Tight Oil Sandstone: A Case Study in the Ordos Basin, China. *J. Pet. Sci. Eng.* **2017**, *149*, 665–674. [CrossRef]
36. Jiu, B.; Huang, W.; Li, Y. An Approach for Quantitative Analysis of Cementation in Sandstone Based on Cathodoluminescence and MATLAB Algorithms. *J. Pet. Sci. Eng.* **2020**, *186*, 106724. [CrossRef]
37. Zhang, Y.; Tian, J.; Zhang, X.; Li, J.; Liang, Q.; Zheng, X. Diagenesis Evolution and Pore Types in Tight Sandstone of Shanxi Formation Reservoir in Hangjinqi Area, Ordos Basin, Northern China. *Energies* **2022**, *15*, 470. [CrossRef]
38. Cao, J.; Hu, W.; Wang, X.; Zhu, D.; Tang, Y.; Xiang, B.; Wu, M. Diagenesis and Elemental Geochemistry under Varying Reservoir Oil Saturation in the Junggar Basin of NW China: Implication for Differentiating Hydrocarbon-Bearing Horizons. *Geofluids* **2015**, *15*, 410–420. [CrossRef]
39. Gao, C.; Ding, X.; Zha, M.; Qu, J. Diagenesis of Unconformity and the Influence on Reservoir Physical Properties: A Case Study of the Lower Jurassic in Xiazijie Area, Junggar Basin, NW China. *J. Petrol. Explor. Prod. Technol.* **2017**, *7*, 659–666. [CrossRef]
40. Tang, Z.; Parnell, J.; Longstaffe, F.J. Diagenesis and Reservoir Potential of Permian–Triassic Fluvial/Lacustrine Sandstones in the Southern Junggar Basin, Northwestern China1. *AAPG Bull.* **1997**, *81*, 1843–1865. [CrossRef]
41. Wang, J.; Zhou, L.; Liu, J.; Zhang, X.; Zhang, F.; Zhang, B. Acid-Base Alternation Diagenesis and Its Influence on Shale Reservoirs in the Permian Lucaogou Formation, Jimusar Sag, Junggar Basin, NW China. *Pet. Explor. Dev.* **2020**, *47*, 962–976. [CrossRef]
42. Wen, H.; Jiang, Y.; Huang, H.; Liu, Y.; Wang, T.; Jiang, Y.; Jin, J.; Qi, L. Provenance and Diagenesis of the Upper Jurassic Qigu Formation Sandstones in the Southern Junggar Basin, NW China. *Arab. J. Geosci.* **2016**, *9*, 452. [CrossRef]
43. Zhou, T.; Wu, C.; Guan, X.; Wang, J.; Jiao, Y. Coupling Relationship between Reservoir Densification and Hydrocarbon Emplacement in the Jurassic Badaowan Formation Sandstone Reservoirs of the Southern Junggar Basin, China. *Geol. J.* **2022**, *57*, 2473–2496. [CrossRef]
44. Bian, W.; Hornung, J.; Liu, Z.; Wang, P.; Hinderer, M. Sedimentary and Palaeoenvironmental Evolution of the Junggar Basin, Xinjiang, Northwest China. *Palaeobio. Palaeoenv.* **2010**, *90*, 175–186. [CrossRef]
45. Hou, H.; Shao, L.; Tang, Y.; Zhao, S.; Yuan, Y.; Li, Y.; Mu, G.; Zhou, Y.; Liang, G.; Zhang, J. Quantitative Characterization of Low-Rank Coal Reservoirs in the Southern Junggar Basin, NW China: Implications for Pore Structure Evolution around the First Coalification Jump. *Mar. Pet. Geol.* **2020**, *113*, 104165. [CrossRef]
46. Fang, Y.; Wu, C.; Guo, Z.; Hou, K.; Dong, L.; Wang, L.; Li, L. Provenance of the Southern Junggar Basin in the Jurassic: Evidence from Detrital Zircon Geochronology and Depositional Environments. *Sediment. Geol.* **2015**, *315*, 47–63. [CrossRef]
47. Guo, H.; Si, X.; Tang, X.; Xu, Y.; Peng, B. Diagenetic Characteristics and Evaluation of Lower-Middle Jurassic Reservoirs in Qigu Fault-Fold Belt, Junggar Basin. *Xinjiang Pet. Geol.* **2020**, *41*, 46–54.
48. Chen, B.; Arakawa, Y. Elemental and Nd-Sr Isotopic Geochemistry of Granitoids from the West Junggar Foldbelt (NW China), with Implications for Phanerozoic Continental Growth. *Geochim. Cosmochim. Acta* **2005**, *69*, 1307–1320. [CrossRef]
49. Zhao, R.; Zhang, J.; Zhou, C.; Zhang, Z.; Chen, S.; Stockli, D.F.; Olariu, C.; Steel, R.; Wang, H. Tectonic Evolution of Tianshan-Bogda-Kelameili Mountains, Clastic Wedge Basin Infill and Chronostratigraphic Divisions in the Source-to-Sink Systems of Permian-Jurassic, Southern Junggar Basin. *Mar. Pet. Geol.* **2020**, *114*, 104200. [CrossRef]
50. Zhou, T.; Wu, C.; Guan, X.; Wang, J.; Zhu, W.; Yuan, B. Effect of Diagenetic Evolution and Hydrocarbon Charging on the Reservoir-Forming Process of the Jurassic Tight Sandstone in the Southern Junggar Basin, NW China. *Energies* **2021**, *14*, 7832. [CrossRef]
51. Tang, S.; Tang, D.; Tao, S.; Sun, B.; Zhang, A.; Zhang, T.; Pu, Y.; Zhi, Y. CO_2-Enriched CBM Accumulation Mechanism for Low-Rank Coal in the Southern Junggar Basin, China. *Int. J. Coal Geol.* **2022**, *253*, 103955. [CrossRef]
52. Brunauer, S.; Emmett, P.H.; Teller, E. Adsorption of Gases in Multimolecular Layers. *J. Am. Chem. Soc.* **1938**, *60*, 309–319. [CrossRef]
53. Barrett, E.P.; Joyner, L.G.; Halenda, P.P. The Determination of Pore Volume and Area Distributions in Porous Substances. I. Computations from Nitrogen Isotherms. *J. Am. Chem. Soc.* **1951**, *73*, 373–380. [CrossRef]

54. Zhou, T.; Wu, C.; Yuan, B.; Shi, Z.; Wang, J.; Zhu, W.; Zhou, Y.; Jiang, X.; Zhao, J.; Wang, J. New Insights into Multiple Provenances Evolution of the Jurassic from Heavy Minerals Characteristics in Southern Junggar Basin, NW China. *Pet. Explor. Dev.* **2019**, *46*, 67–81. [CrossRef]
55. Xi, K.; Cao, Y.; Haile, B.G.; Zhu, R.; Jahren, J.; Bjørlykke, K.; Zhang, X.; Hellevang, H. How Does the Pore-Throat Size Control the Reservoir Quality and Oiliness of Tight Sandstones? The Case of the Lower Cretaceous Quantou Formation in the Southern Songliao Basin, China. *Mar. Pet. Geol.* **2016**, *76*, 1–15. [CrossRef]
56. Zhang, L.; Lu, S.; Xiao, D.; Li, B. Pore Structure Characteristics of Tight Sandstones in the Northern Songliao Basin, China. *Mar. Pet. Geol.* **2017**, *88*, 170–180. [CrossRef]
57. Lundegard, P.D. Sandstone Porosity Loss: A "Big Picture" View of the Importance of Compaction. *J. Sediment. Res.* **1992**, *62*, 250–260. [CrossRef]
58. Ramm, M. Porosity-Depth Trends in Reservoir Sandstones: Theoretical Models Related to Jurassic Sandstones Offshore Norway. *Mar. Pet. Geol.* **1992**, *9*, 553–567. [CrossRef]
59. Holland, H.D.; Mackenzie, F.T.; Turekian, K.K. *Sediments, Diagenesis, and Sedimentary Rocks: Treatise on Geochemistry*, 2nd ed.; Elsevier Science: Amsterdam, The Netherlands, 2005; Volume 7, ISBN 978-0-08-044849-7.
60. Xi, K.; Cao, Y.; Jahren, J.; Zhu, R.; Bjørlykke, K.; Zhang, X.; Cai, L.; Hellevang, H. Quartz Cement and Its Origin in Tight Sandstone Reservoirs of the Cretaceous Quantou Formation in the Southern Songliao Basin, China. *Mar. Pet. Geol.* **2015**, *66*, 748–763. [CrossRef]
61. Gier, S.; Worden, R.H.; Krois, P. Comparing Clay Mineral Diagenesis in Interbedded Sandstones and Mudstones, Vienna Basin, Austria. *Geol. Soc. Lond. Spec. Publ.* **2018**, *435*, 389–403. [CrossRef]
62. Mozley, P.S.; Heath, J.E.; Dewers, T.A.; Bauer, S.J. Origin and Heterogeneity of Pore Sizes in the Mount Simon Sandstone and Eau Claire Formation: Implications for Multiphase Fluid Flow. *Geosphere* **2016**, *12*, 1341–1361. [CrossRef]
63. Salem, A.M.; Ketzer, J.M.; Morad, S.; Rizk, R.R.; Al-Aasm, I.S. Diagenesis and Reservoir-Quality Evolution of Incised-Valley Sandstones: Evidence from the Abu Madi Gas Reservoirs (Upper Miocene), the Nile Delta Basin, Egypt. *J. Sediment. Res.* **2005**, *75*, 572–584. [CrossRef]
64. Xi, K.; Cao, Y.; Liu, K.; Wu, S.; Yuan, G.; Zhu, R.; Kashif, M.; Zhao, Y. Diagenesis of Tight Sandstone Reservoirs in the Upper Triassic Yanchang Formation, Southwestern Ordos Basin, China. *Mar. Pet. Geol.* **2019**, *99*, 548–562. [CrossRef]
65. Jiu, B.; Huang, W.; Li, Y.; He, M. Influence of Clay Minerals and Cementation on Pore Throat of Tight Sandstone Gas Reservoir in the Eastern Ordos Basin, China. *J. Nat. Gas. Sci. Eng.* **2021**, *87*, 103762. [CrossRef]
66. Yuan, G.; Gluyas, J.; Cao, Y.; Oxtoby, N.H.; Jia, Z.; Wang, Y.; Xi, K.; Li, X. Diagenesis and Reservoir Quality Evolution of the Eocene Sandstones in the Northern Dongying Sag, Bohai Bay Basin, East China. *Mar. Pet. Geol.* **2015**, *62*, 77–89. [CrossRef]
67. Vincent, B.; van Buchem, F.S.P.; Bulot, L.G.; Jalali, M.; Swennen, R.; Hosseini, A.S.; Baghbani, D. Depositional Sequences, Diagenesis and Structural Control of the Albian to Turonian Carbonate Platform Systems in Coastal Fars (SW Iran). *Mar. Pet. Geol.* **2015**, *63*, 46–67. [CrossRef]
68. Wang, Q.; Xu, H.; Tang, D.; Yang, S.; Wang, G.; Ren, P.; Dong, W.; Guo, J. Indication of Origin and Distribution of Coalbed Gas from Stable Isotopes of Gas and Coproduced Water in Fukang Area of Junggar Basin, China. *AAPG Bull.* **2022**, *106*, 387–407. [CrossRef]
69. Lai, J.; Wang, G.; Ran, Y.; Zhou, Z.; Cui, Y. Impact of Diagenesis on the Reservoir Quality of Tight Oil Sandstones: The Case of Upper Triassic Yanchang Formation Chang 7 Oil Layers in Ordos Basin, China. *J. Pet. Sci. Eng.* **2016**, *145*, 54–65. [CrossRef]
70. Bjorlykke, K. *Petroleum Geoscience: From Sedimentary Environments to Rock Physics*; Springer Science & Business Media: Berlin/Heidelberg, Germany, 2010; ISBN 978-3-642-02332-3.
71. Dias, R.F.; Freeman, K.H.; Lewan, M.D.; Franks, S.G. Δ13C of Low-Molecular-Weight Organic Acids Generated by the Hydrous Pyrolysis of Oil-Prone Source Rocks. *Geochim. Cosmochim. Acta* **2002**, *66*, 2755–2769. [CrossRef]
72. Schmid, S.; Worden, R.H.; Fisher, Q.J. Diagenesis and Reservoir Quality of the Sherwood Sandstone (Triassic), Corrib Field, Slyne Basin, West of Ireland. *Mar. Pet. Geol.* **2004**, *21*, 299–315. [CrossRef]
73. Freiburg, J.T.; Ritzi, R.W.; Kehoe, K.S. Depositional and Diagenetic Controls on Anomalously High Porosity within a Deeply Buried CO_2 Storage Reservoir—The Cambrian Mt. Simon Sandstone, Illinois Basin, USA. *Int. J. Greenh. Gas. Control.* **2016**, *55*, 42–54. [CrossRef]
74. Ehrenberg, S.N. Relationship Between Diagenesis and Reservoir Quality in Sandstones of the Garn Formation, Haltenbanken, Mid-Norwegian Continental Shelf1. *AAPG Bull.* **1990**, *74*, 1538–1558. [CrossRef]
75. Sborne, M.J.; Swarbrick, R.E. Diagenesis in North Sea HPHT Clastic Reservoirs—Consequences for Porosity and Overpressure Prediction. *Mar. Pet. Geol.* **1999**, *16*, 337–353. [CrossRef]
76. Blatt, H. Diagenetic Processes in Sandstones. In *Aspects of Diagenesis*; Scholle, P.A., Schluger, P.R., Eds.; SEPM Society for Sedimentary Geology, Special Publication: Tulsa, OK, USA, 1979; pp. 141–157.
77. McBride, E.F. Quartz Cement in Sandstones: A Review. *Earth Sci. Rev.* **1989**, *26*, 69–112. [CrossRef]
78. Yan, J.; Liu, C.; Zhang, W.; Li, B. Diagenetic Characteristics of the Lower Porosity and Permeability Sandstones of the Upper Paleozoic in the South of Ordos Basin. *Acta Geol. Sin.* **2010**, *84*, 272–279.
79. Kantorowicz, J.D. The Influence of Variations in Illite Morphology on the Permeability of Middle Jurassic Brent Group Sandstones, Cormorant Field, UK North Sea. *Mar. Pet. Geol.* **1990**, *7*, 66–74. [CrossRef]

80. Gaupp, R.; Matter, A.; Platt, J.; Ramseyer, K.; Walzebuck, J. Diagenesis and Fluid Evolution of Deeply Buried Permian (Rotliegende) Gas Reservoirs, Northwest Germany1. *AAPG Bull.* **1993**, *77*, 1111–1128. [CrossRef]
81. Towe, K.M. Clay Mineral Diagenesis as a Possible Source of Silica Cement in Sedimentary Rocks. *J. Sediment. Res.* **1962**, *32*, 26–28. [CrossRef]
82. Boles, J.R.; Franks, S.G. Clay Diagenesis in Wilcox Sandstones of Southwest Texas; Implications of Smectite Diagenesis on Sandstone Cementation. *J. Sediment. Res.* **1979**, *49*, 55–70. [CrossRef]
83. Ronald, C.S.; Crossey, L.J.; Hagen, E.S.; Heasler, H.P. Organic-Inorganic Interactions and Sandstone Diagenesis1. *AAPG Bull.* **1989**, *73*, 1–23. [CrossRef]
84. Tao, S.; Gao, X.; Li, C.; Zeng, J.; Zhang, X.; Yang, C.; Zhang, J.; Gong, Y. The Experimental Modeling of Gas Percolation Mechanisms in a Coal-Measure Tight Sandstone Reservoir: A Case Study on the Coal-Measure Tight Sandstone Gas in the Upper Triassic Xujiahe Formation, Sichuan Basin, China. *J. Nat. Gas. Geosci.* **2016**, *1*, 445–455. [CrossRef]
85. Rahman, M.J.J.; Worden, R.H. Diagenesis and Its Impact on the Reservoir Quality of Miocene Sandstones (Surma Group) from the Bengal Basin, Bangladesh. *Mar. Pet. Geol.* **2016**, *77*, 898–915. [CrossRef]
86. Grigsby, J.D. Origin and Growth Mechanism of Authigenic Chlorite in Sandstones of the Lower Vicksburg Formation, South Texas. *J. Sediment. Res.* **2001**, *71*, 27–36. [CrossRef]
87. Virolle, M.; Brigaud, B.; Luby, S.; Portier, E.; Féniès, H.; Bourillot, R.; Patrier, P.; Beaufort, D. Influence of Sedimentation and Detrital Clay Grain Coats on Chloritized Sandstone Reservoir Qualities: Insights from Comparisons between Ancient Tidal Heterolithic Sandstones and a Modern Estuarine System. *Mar. Pet. Geol.* **2019**, *107*, 163–184. [CrossRef]
88. Yao, J.L.; Wang, Q.; Zhang, R.; Li, S.T. Forming Mechanism and Their Environmental Implications of Chlorite-Coatings in Chang 6 Sandstone (Upper Triassic) of Hua-Qing Area, Ordos Basin. *Acta Sedimentol. Sin.* **2011**, *29*, 72–79.
89. Midtbø, R.E.A.; Rykkje, J.M.; Ramm, M. Deep Burial Diagenesis and Reservoir Quality along the Eastern Flank of the Viking Graben. Evidence for Illitization and Quartz Cementation after Hydrocarbon Emplacement. *Clay Miner.* **2000**, *35*, 227–237. [CrossRef]
90. Baker, J.C. Diagenesis and Reservoir Quality of the Aldebaran Sandstone, Denison Trough, East-Central Queensland, Australia. *Sedimentology* **1991**, *38*, 819–838. [CrossRef]
91. Littke, R.; Zieger, L. Deposition, Diagenesis and Petroleum Generation Potential of Pennsylvanian Coals and Coal-Bearing Strata in Western Germany: A Review. *Z. Der Dtsch. Ges. Für Geowiss.* **2019**, *170*, 289–309. [CrossRef]
92. Zhou, Y.; Ji, Y.; Xu, L.; Che, S.; Niu, X.; Wan, L.; Zhou, Y.; Li, Z.; You, Y. Controls on Reservoir Heterogeneity of Tight Sand Oil Reservoirs in Upper Triassic Yanchang Formation in Longdong Area, Southwest Ordos Basin, China: Implications for Reservoir Quality Prediction and Oil Accumulation. *Mar. Pet. Geol.* **2016**, *78*, 110–135. [CrossRef]
93. Nguyen, D.; Horton, R.A.; Kaess, A.B. Diagenesis of the Oligocene Vedder Formation, Greeley Oil Field, Southern San Joaquin Basin, California. In Proceedings of the Pacific Section AAPG, SPE and SEPM Joint Technical Conference, Bakersfield, CA, USA, 29 April 2014.
94. Beard, D.C.; Weyl, P.K. Influence of Texture on Porosity and Permeability of Unconsolidated Sand1. *AAPG Bull.* **1973**, *57*, 349–369. [CrossRef]
95. Ramm, M. Reservoir Quality and Its Relationship to Facies and Provenance in Middle to Upper Jurassic Sequences, Northeastern North Sea. *Clay Miner.* **2000**, *35*, 77–94. [CrossRef]
96. Rezaee, R. *Fundamentals of Gas Shale Reservoirs*; John Wiley & Sons: Hoboken, NJ, USA, 2015; ISBN 978-1-118-64579-6.
97. Ehrenberg, S.N. Influence of Depositional Sand Quality and Diagenesis on Porosity and Permeability; Examples from Brent Group Reservoirs, Northern North Sea. *J. Sediment. Res.* **1997**, *67*, 197–211. [CrossRef]
98. Lai, J.; Wang, G.; Ran, Y.; Zhou, Z. Predictive Distribution of High-Quality Reservoirs of Tight Gas Sandstones by Linking Diagenesis to Depositional Facies: Evidence from Xu-2 Sandstones in the Penglai Area of the Central Sichuan Basin, China. *J. Nat. Gas. Sci. Eng.* **2015**, *23*, 97–111. [CrossRef]
99. Fisher, Q.J.; Casey, M.; Clennell, M.B.; Knipe, R.J. Mechanical Compaction of Deeply Buried Sandstones of the North Sea. *Mar. Pet. Geol.* **1999**, *16*, 605–618. [CrossRef]
100. Rossi, C.; Marfil, R.; Ramseyer, K.; Permanyer, A. Facies-Related Diagenesis and Multiphase Siderite Cementation and Dissolution in the Reservoir Sandstones of the Khatatba Formation, Egypt's Western Desert. *J. Sediment. Res.* **2001**, *71*, 459–472. [CrossRef]
101. Zhu, R.; Zou, C.; Zhang, N.; Wang, X.; Cheng, R.; Liu, L.; Zhou, C.; Song, L. Diagenetic Fluids Evolution and Genetic Mechanism of Tight Sandstone Gas Reservoirs in Upper Triassic Xujiahe Formation in Sichuan Basin, China. *Sci. China Ser. D-Earth Sci.* **2008**, *51*, 1340–1353. [CrossRef]
102. Zou, C.; Zhu, R.; Liu, K.; Su, L.; Bai, B.; Zhang, X.; Yuan, X.; Wang, J. Tight Gas Sandstone Reservoirs in China: Characteristics and Recognition Criteria. *J. Pet. Sci. Eng.* **2012**, *88–89*, 82–91. [CrossRef]
103. Ji, Y.; Zhou, Y.; Liu, Y.; Lu, H.; Liu, Q.; Wang, Y. The Impact of Sedimentary Characteristics on the Diagenesis and Reservoir Quality of the 1st Member of Paleogene Funing Formation in the Gaoyou Subbasin. *Acta Geol. Sin.* **2014**, *88*, 1299–1310.
104. Wu, H.; Ji, Y.; Liu, R.; Zhang, C.; Chen, S. Insight into the Pore Structure of Tight Gas Sandstones: A Case Study in the Ordos Basin, NW China. *Energy Fuels* **2017**, *31*, 13159–13178. [CrossRef]